

A novel finite element formulation for static bending analysis of functionally graded porous sandwich plates

Van Chinh NGUYEN^a, Trung Thanh TRAN^a, Trung NGUYEN-THOI^{b,c}, Quoc-Hoa PHAM^{d*}

^a Faculty of Mechanical Engineering, Le Quy Don Technical University, Hanoi, Vietnam

^b Laboratory for Applied and Industrial Mathematics, Institute for Computational Science and Artificial Intelligence, Van Lang University, Ho Chi Minh City, Vietnam

^c Faculty of Mechanical-Electrical and Computer Engineering, Van Lang University, Ho Chi Minh City, Vietnam

^d Faculty of Engineering and Technology, Nguyen Tat Thanh University, Ho Chi Minh City, Vietnam

*Corresponding author. E-mail: pqhoa@ntt.edu.vn

© Higher Education Press 2022

ABSTRACT This article aims to propose a finite element formulation based on Quasi-3D theory for the static bending analysis of functionally graded porous (FGP) sandwich plates. The FGP sandwich plates consist of three layers including the bottom skin of homogeneous metal, the top skin of fully ceramic and the FGP core layer with uneven porosity distribution. A quadrilateral (Q4) element with nine degrees of freedom (DOFs) per node is derived and employed in analyzing the static bending response of the plate under uniform and/or sinusoidally distributed loads. The accuracy of the present finite element formulation is verified by comparing the obtained numerical results with the published results in the literature. Then, some numerical examples are performed to examine the effects of the parameters including power-law index k and porosity coefficient ξ on the static bending response of rectangular FGP sandwich plates. In addition, a problem with a complicated L-shape model is conducted to illustrate the superiority of the proposed finite element method.

KEYWORDS sandwich plates, functionally graded porous, static bending, Quasi-3D theory, Q4 element

1 Introduction

Functionally graded materials (FGMs) were first studied by Japanese scientists in 1984 at Sendai Institute. These materials are made of two or more component materials, usually ceramic and metal in which material properties vary smoothly and continuously from one surface to the other one. They have many outstanding features compared to traditional materials, such as high-temperature resistance, good corrosion resistance, etc. Therefore, FGMs have been applied in high-tech fields such as aerospace engineering, nuclear power, biology and so on. The outstanding characteristics of FGMs can eliminate stress concentration and delamination phenomena which often occur in laminated composite materials. The initial studies on behavior analysis of structures using FGMs

can be summarized as those involved with beams [1–4], plates [5–25] and shells [26–28]. Functionally graded porous (FGP) material is a form of FGMs including many pores that develop in the process of making the material. This material possesses several outstanding mechanical properties such as low density, excellent energy-absorbing capability, great thermal resistant properties, etc. They have been widely applied in various fields including aerospace, automotive industry, and civil engineering. Some works on the mechanical behavior of structures using FGP are as follows. Rezaei and Saidi [29,30] used the exact solutions to analyze the vibration of porous-cellular plates. Zhao et al. [31,32] employed an improved Fourier method to examine the bending and dynamical response of FGP doubly-curved panels and shells. Li et al. [33] analyzed the free vibration and dynamic buckling behavior of sandwich FGP plate reinforced GPL for nonlinear problems, and Sahmani

et al. [34] studied large-amplitude vibrations of FGP micro/nano-plates. Gou et al. [35,36] used the deep collocation method based on neuron architecture search-and-transfer learning for heterogeneous porous materials. Readers can see the application of artificial intelligence (AI) in scientific and mechanical problems for plate and shell structures in [37–39]. In general, almost the above works are based on analytical solutions, so they are limited in terms of models, loads and boundary conditions.

Sandwich structures are basically fabricated by attaching two thin skins to a thick lightweight core. Recently, sandwich structures have been used popularly in aerospace vehicles due to their outstanding bending rigidity, low mass density, good noise cancellation and insulation. However, they are highly susceptible to failure due to stress concentration at load areas, and due to geometrical and material discontinuities of sandwich plates. Some researchers have studied the static bending, buckling and free vibration behavior of the functionally graded material (FGM) plates, employing refined plate theories. Specifically, Zenkour et al. [40–49] uses analytical solutions with many improvements in plate theory to obtain accurate results in the problems of analyzing bending and stress [40,41], mechanical and thermal bending [42–45], free vibration and buckling [46,47], and the effect of porosity [48,49]. Thai et al. [50] used a new first-order shear deformation theory (FSDT), while Sid Ahmed Houari et al. [51] refined a higher-order shear deformation theory (HSDT). Nguyen et al. [52,53] developed a smoothed finite element method for the mixed interpolation of tensorial components technique of triangular elements (MITC3). Li et al. [54,55] employed the Navier approach, while Tounsi et al. [56] developed a refined trigonometric shear deformation theory. In addition, Tlidji et al. [57] used an analytical method to study behavior of FGM sandwich plates. Using Quasi-3D theory, some typical works can be mentioned as follows. Zaoui et al. [58] used two different shear deformation theories (2D, Quasi-3D) and Navier solutions to analyze the vibrations response of FGM plate on elastic foundation. Neves et al. [59] used a meshless technique based on sinusoidal Quasi-3D deformation theory to study the static bending, free vibration, and stability of FGM sandwich plate. Farzam-Rad et al. [60] used Quasi-3D shear deformation theory and isogeometric analysis for the static and free vibration analysis of FGM sandwich plate with attention to the physical neutral surface position. Vafakhah and Navayi Neya [61] proposed an accurate solution for the static bending problems of simple support rectangular FGM thick plates with 3D model.

Use of the quadrilateral (Q4) element is straightforward and achieves initial results in analyzing the mechanical behavior of structures. However, using only five degrees of freedom (DOFs) per node based on the Lagrange interpolations with a shear correction factor still does not

satisfy the stress-free condition at the upper and lower boundaries of plates. In addition, the above-mentioned literature reveals that there is still a research gap for proposing new effective finite element formulations for analysis of FGP sandwich plates. The work is therefore conducted to fill in this research gap by proposing a new finite element formulation using the Q4 element with nine DOFs per node based on the combination of the Lagrange interpolations and the Hermit interpolations to establish the governing equation of FGP sandwich plates. Then, a few examples are examined to explore the accuracy and reliability of the proposed method. Moreover, the numerical and graphical results help to demonstrate the effect of geometrical parameters and material properties on the static bending of FGP sandwich plates.

This article is organized as follows. Section 1 presents a general introduction and literature review. Sections 2 and 3 provide the finite element formulations based on Quasi-3D theory for static bending analysis of FGP sandwich plates. Section 4 demonstrates the numerical results and discussion. Finally, Section 5 gives major conclusions.

2 The functionally graded porous sandwich plate

In this paper, the FGP sandwich plate as shown in Fig. 1 is considered.

In Fig. 1, a , b , and h are the length, width, and thickness dimensions of sandwich plates, respectively. The sandwich plate structure consists of the FGP core layer, a bottom layer of homogeneous metal, and a fully ceramic top layer. The ceramic volume fraction V_c^n ($n = 1, 2, 3$) in the layers, i.e., the bottom layer, the core layer and the top layer are determined according to power-law function [48]:

$$\begin{cases} V_c^1(z) = 0, & z \in \left[\frac{-h}{2}; h_1 \right], \\ V_c^2(z) = \left(\frac{z - h_1}{h_2 - h_1} \right)^k, & z \in [h_1; h_2], \\ V_c^3(z) = 1, & z \in \left[h_2; \frac{h}{2} \right], \end{cases} \quad (1)$$

where k represents the power-law index; z is the integral variable according to the plate thickness.

The metal volume fraction in the layers is inferred by the formula:

$$V_m^n(z) = 1 - V_c^n(z). \quad (2)$$

The core layer is made by FGP material with uneven porosity distribution expressed by the rule of the mixture as follows:

$$P^2(z) = P_m^2 + (P_c^2 - P_m^2) V_c^2 - \frac{\xi}{2} \left(1 - \frac{2|z|}{h} \right) (P_m^2 + P_c^2), \quad (3)$$

where P represents the effective material properties such as elastic modulus E , mass density ρ , and Poisson's ratio ν ; subscripts 'm' and 'c' denote the metal and ceramic constituents, respectively; ξ is the porosity coefficient.

Besides, Fig. 2 plots the effective elastic modulus through thickness with different values of k and thickness ratio between the bottom layer, the core layer and the top layer (so-called scheme h_b - h_c - h_t) with mechanical properties as shown in Table 1. Herein, scheme 0-1-0

corresponds to the case of isotropic FGP plates.

3 Theoretical formulation

3.1 The Quasi-3D theory for functionally graded porous sandwich plates

According to Quasi-3D theory, the displacement field of

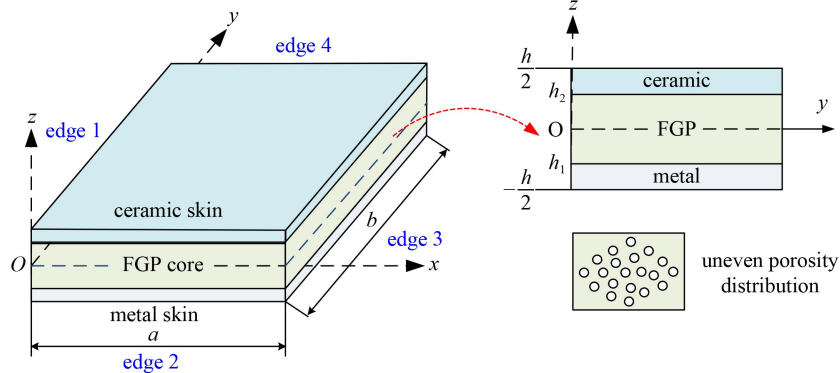


Fig. 1 The schematic diagram for the geometry of the FGP sandwich plate.

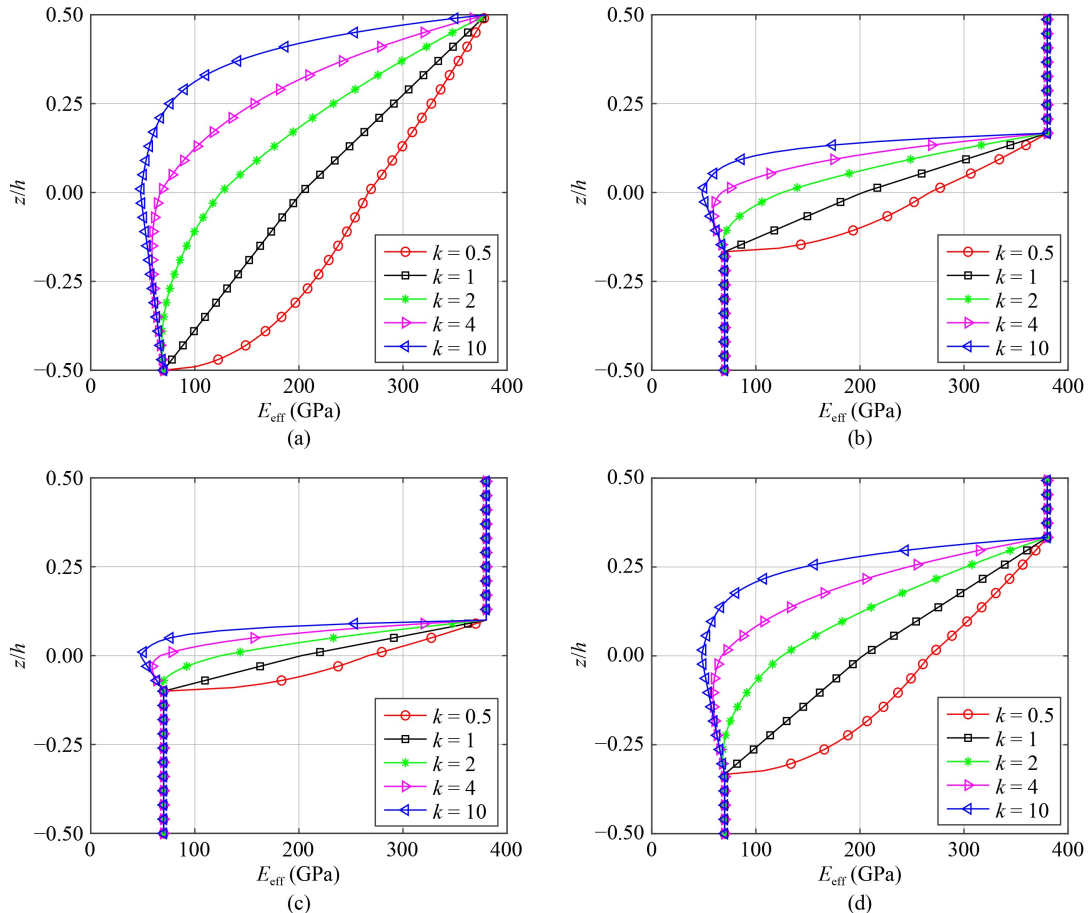


Fig. 2 Effective elastic modulus of FGP sandwich plates through the thickness ($\xi = 0.1$). (a) Scheme 0-1-0; (b) scheme 1-1-1; (c) scheme 2-1-2; (d) scheme 1-4-1.

Table 1 Mechanical properties of the constituent materials

material properties	Young's moduli (GPa)	mass densities (kg/m ³)	Poisson's ratio
alumina (Al_2O_3) (ceramic)	$E_c = 380$	$\rho_c = 3800$	$\nu_c = 0.3$
aluminum (Al) (metal)	$E_m = 70$	$\rho_m = 2707$	$\nu_m = 0.3$

FGP sandwich plates can be expressed as follows [62]:

$$\begin{cases} u(x, y, z) = u_0(x, y, 0) - zw_{b,x} - f(z)w_{s,x}, \\ v(x, y, z) = v_0(x, y, 0) - zw_{b,y} - f(z)w_{s,y}, \\ w(x, y, z) = w_b + w_s + g(z)w_z, \end{cases} \quad (4)$$

where u_0 , v_0 , w_b , w_s , and w_z are displacements variables in the neutral plane at the point (x, y, z) . $f(z) = \frac{4z^3}{3h^2}$; $g(z) = 1 - \frac{4z^2}{h^2}$ are the continuous functions [63]. Note that $f(z)$ is the continuous function that is established basing on three following rules: 1) the function must be continuous; 2) the deformed surface is curved; and 3) the stress-free condition at the upper and lower boundaries of the plate is satisfied.

Recently, many continuum functions $f(z)$ have been created by scientists all over the world [64–68]. In this work, the Reddy's continuous function is chosen due to its proven efficiency and simple polynomial. Besides, the current authors' previous studies regarding the performance of these functions [69] illustrated that using different functions can affect the numerical performance. It should be noted that the new component $g(z)w_z$ in Eq. (4) is added to investigate the thickness stretching effect on the static bending of FGP sandwich plates.

Then, the strain components are inferred from the displacement field as follows:

$$\begin{aligned} \boldsymbol{\varepsilon} &= \begin{Bmatrix} \boldsymbol{\varepsilon}_1 \\ 0 \end{Bmatrix} + \begin{Bmatrix} 0 \\ \boldsymbol{\varepsilon}_2 \end{Bmatrix}, \\ \boldsymbol{\varepsilon}_1 &= \begin{Bmatrix} \varepsilon_x & \varepsilon_y & \varepsilon_z & \gamma_{xy} \end{Bmatrix}^T, \\ \boldsymbol{\varepsilon}_2 &= \begin{Bmatrix} \gamma_{yz} & \gamma_{xz} \end{Bmatrix}^T, \end{aligned} \quad (5a)$$

where

$$\begin{aligned} \boldsymbol{\varepsilon}_1 &= \boldsymbol{\varepsilon}_m + z\boldsymbol{\kappa}_b + f(z)\boldsymbol{\kappa}_s + g_z\boldsymbol{\varepsilon}_z, \\ \boldsymbol{\varepsilon}_2 &= g(z)\boldsymbol{\varepsilon}_{s1} + g(z)\boldsymbol{\varepsilon}_{s2}, \\ \boldsymbol{\varepsilon}_m &= \begin{Bmatrix} u_{0,x} & v_{0,y} & 0 & (u_{0,y} + v_{0,x}) \end{Bmatrix}^T, \\ \boldsymbol{\kappa}_b &= -\begin{Bmatrix} w_{b,xx} & w_{b,yy} & 0 & 2w_{b,xy} \end{Bmatrix}^T, \\ \boldsymbol{\kappa}_s &= -\begin{Bmatrix} w_{s,xx} & w_{s,yy} & 0 & 2w_{s,xy} \end{Bmatrix}^T, \\ \boldsymbol{\varepsilon}_z &= \begin{Bmatrix} 0 & 0 & w_z & 0 \end{Bmatrix}^T, \\ \boldsymbol{\varepsilon}_{s1} &= \begin{Bmatrix} w_{s,y} & w_{s,x} \end{Bmatrix}^T, \\ \boldsymbol{\varepsilon}_{s2} &= \begin{Bmatrix} w_{z,y} & w_{z,x} \end{Bmatrix}^T. \end{aligned} \quad (5b)$$

From Hooke's law, the stress-strain relation is:

$$\begin{aligned} \boldsymbol{\sigma} &= \begin{Bmatrix} \sigma_1 \\ 0 \end{Bmatrix} + \begin{Bmatrix} 0 \\ \boldsymbol{\sigma}_2 \end{Bmatrix}, \\ \boldsymbol{\sigma}_1 &= \begin{Bmatrix} \sigma_x & \sigma_y & \sigma_z & \tau_{xy} \end{Bmatrix}^T = \mathbf{D}_1 \boldsymbol{\varepsilon}_1, \\ \boldsymbol{\sigma}_2 &= \begin{Bmatrix} \tau_{yz} & \tau_{xz} \end{Bmatrix}^T = \mathbf{D}_2 \boldsymbol{\varepsilon}_2, \end{aligned} \quad (6a)$$

in which

$$\begin{aligned} \mathbf{D}_1 &= E(z) \begin{bmatrix} a_1 & a_2 & a_2 & 0 \\ a_2 & a_1 & a_2 & 0 \\ a_2 & a_2 & a_1 & 0 \\ 0 & 0 & 0 & a_3 \end{bmatrix}, \\ \mathbf{D}_2 &= E(z) \begin{bmatrix} a_3 & 0 \\ 0 & a_3 \end{bmatrix}, \end{aligned}$$

$$\begin{aligned} a_1 &= \frac{1 - \nu(z)^2}{1 - 3\nu(z)^2 - 2\nu(z)^3}, \\ a_2 &= \frac{\nu(z)(1 + \nu(z))}{1 - 3\nu(z)^2 - 2\nu(z)^3}, \\ a_3 &= \frac{1}{2(1 + \nu(z))}. \end{aligned} \quad (6b)$$

The strain energy is calculated by:

$$U = \frac{1}{2} \int_V \boldsymbol{\varepsilon}^T \boldsymbol{\sigma} dV = \frac{1}{2} \int_V (\boldsymbol{\varepsilon}_1^T \boldsymbol{\sigma}_1 + \boldsymbol{\varepsilon}_2^T \boldsymbol{\sigma}_2) dV, \quad (7)$$

where V is the volume of the sandwich plate. When the sandwich plate is affected by the distribution load $q(x, y)$, which is perpendicular to the neutral plane of the sandwich plate, the work done by the external force is determined by

$$W = \int_{\Omega} (w_b + w_s + w_z) q(x, y) d\Omega, \quad (8)$$

in which Ω is the neutral plane area of the sandwich plate.

3.2 Finite element formulation

Using the Q4 element with 36 DOFs (each node with nine DOFs) to discretize the model of the FGP sandwich plate (Fig. 3). The node displacement vector of the element is defined as follows:

$$\mathbf{d}_e = \left[\mathbf{d}_m^T \quad \mathbf{d}_b^T \quad \mathbf{d}_s^T \quad \mathbf{d}_z^T \right]_{36 \times 1}^T, \quad (9)$$

herein

$$\begin{aligned}
\mathbf{d}_m &= \left\{ \begin{matrix} \mathbf{d}_u^T & \mathbf{d}_v^T \end{matrix} \right\}^T, \quad \mathbf{d}_u = \left\{ \begin{matrix} u_{01} & u_{02} & u_{03} & u_{04} \end{matrix} \right\}^T, \\
\mathbf{d}_v &= \left\{ \begin{matrix} v_{01} & v_{02} & v_{03} & v_{04} \end{matrix} \right\}^T, \\
\mathbf{d}_b &= \left\{ \begin{matrix} \Delta_{b1}^T & \Delta_{b2}^T & \Delta_{b3}^T & \Delta_{b4}^T \end{matrix} \right\}^T, \\
\mathbf{A}_{bi} &= \left\{ \begin{matrix} w_{bi} & w_{b,xi} & w_{b,yi} \end{matrix} \right\}^T, \\
\mathbf{A}_{si} &= \left\{ \begin{matrix} w_{si} & w_{s,xi} & w_{s,yi} \end{matrix} \right\}^T, \\
\mathbf{d}_s &= \left\{ \begin{matrix} \Delta_{s1}^T & \Delta_{s2}^T & \Delta_{s3}^T & \Delta_{s4}^T \end{matrix} \right\}^T, \\
\mathbf{A}_{si} &= \left\{ \begin{matrix} w_{si} & w_{s,xi} & w_{s,yi} \end{matrix} \right\}^T, \quad (i = 1, \dots, 4) \\
\mathbf{d}_z &= \left\{ \begin{matrix} w_{z1} & w_{z2} & w_{z3} & w_{z4} \end{matrix} \right\}^T. \tag{10}
\end{aligned}$$

The node displacement components of the element are defined by

$$u_0 = \mathbf{N}\mathbf{d}_u, v_0 = \mathbf{N}\mathbf{d}_v, w_b = \mathbf{H}\mathbf{d}_b, w_s = \mathbf{H}\mathbf{d}_s, w_z = \mathbf{N}\mathbf{d}_z, \quad (11)$$

with $\mathbf{N} = [N_1 \ N_2 \ N_3 \ N_4]$, $\mathbf{H} = [H_1 \ H_2 \ \dots \ H_{12}]$ are Lagrange and the Hermit interpolations given by

$$\begin{cases} N_1 = \frac{1}{4}(1-r)(1-s), \ N_2 = \frac{1}{4}(1+r)(1-s), \\ N_3 = \frac{1}{4}(1+r)(1+s), \ N_4 = \frac{1}{4}(1-r)(1+s), \end{cases} \tag{12a}$$

and

$$\begin{cases} H_1 = \frac{1}{8}(1-r)(1-s)(2-r-s-r^2-s^2), \\ H_2 = \frac{1}{8}(1-r)(1-s)(1-r^2), \\ H_3 = \frac{1}{8}(1-r)(1-s)(1-s^2), \\ H_4 = \frac{1}{8}(1+r)(1-s)(2+r-s-r^2-s^2), \\ H_5 = -\frac{1}{8}(1+r)(1-s)(1-r^2), \\ H_6 = \frac{1}{8}(1+r)(1-s)(1-r^2), \\ H_7 = \frac{1}{8}(1+r)(1+s)(2+r+s-r^2-s^2), \\ H_8 = -\frac{1}{8}(1+r)(1+s)(1-r^2), \\ H_9 = -\frac{1}{8}(1+r)(1+s)(1-s^2), \\ H_{10} = \frac{1}{8}(1-r)(1+s)(2-r+s-r^2-s^2), \\ H_{11} = \frac{1}{8}(1-r)(1+s)(1-r^2), \\ H_{12} = -\frac{1}{8}(1-r)(1+s)(1-s^2), \end{cases} \tag{12b}$$

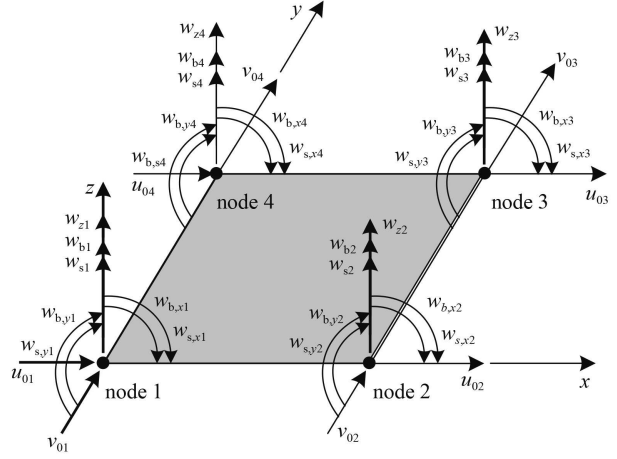


Fig. 3 Model of Q4 element with nine DOFs per node.

Substituting Eq. (11) into Eq. (5b), we get the strain vector as follows.

$$\begin{aligned} \boldsymbol{\epsilon}_m &= \mathbf{B}_m \mathbf{d}_m, \quad \boldsymbol{\kappa}_b = \mathbf{C}_b \mathbf{d}_b, \quad \boldsymbol{\kappa}_s = \mathbf{C}_s \mathbf{d}_s, \\ \boldsymbol{\epsilon}_z &= \mathbf{B}_z \mathbf{d}_z, \quad \boldsymbol{\epsilon}_{s1} = \mathbf{B}_{s1} \mathbf{d}_s, \quad \boldsymbol{\epsilon}_{s2} = \mathbf{B}_{s2} \mathbf{d}_z, \end{aligned} \tag{13}$$

where

$$\begin{aligned} \mathbf{B}_m &= \begin{bmatrix} \mathbf{N}_{,x} & \mathbf{0} \\ \mathbf{0} & \mathbf{N}_{,y} \\ \mathbf{0} & \mathbf{0} \\ \mathbf{N}_{,y} & \mathbf{N}_{,x} \end{bmatrix}, \quad \mathbf{C}_b = \mathbf{C}_s = - \begin{bmatrix} \mathbf{H}_{,xx} \\ \mathbf{H}_{,yy} \\ \mathbf{0} \\ 2\mathbf{H}_{,xy} \end{bmatrix}, \\ \mathbf{B}_z &= \begin{bmatrix} \mathbf{0} \\ \mathbf{0} \\ N \\ \mathbf{0} \end{bmatrix}, \quad \mathbf{B}_{s1} = \begin{bmatrix} \mathbf{H}_{,y} \\ \mathbf{H}_{,x} \end{bmatrix}, \quad \mathbf{B}_{s2} = \begin{bmatrix} \mathbf{N}_{,y} \\ \mathbf{N}_{,x} \end{bmatrix}. \end{aligned} \tag{14}$$

Substituting Eq. (13) into Eq. (5b) and combining with Eq. (7), the strain energy of element sandwich plates is obtained as follows.

$$U_e = \frac{1}{2} \mathbf{d}_e^T \mathbf{K}_e \mathbf{d}_e = \frac{1}{2} \mathbf{d}_e^T \begin{bmatrix} \mathbf{k}_{mm} & \mathbf{k}_{mb} & \mathbf{k}_{ms} & \mathbf{k}_{mz} \\ \mathbf{k}_{mb}^T & \mathbf{k}_{bb} & \mathbf{k}_{bs} & \mathbf{k}_{bz} \\ \mathbf{k}_{ms}^T & \mathbf{k}_{bs}^T & \mathbf{k}_{ss} & \mathbf{k}_{sz} \\ \mathbf{k}_{mz}^T & \mathbf{k}_{bz}^T & \mathbf{k}_{sz}^T & \mathbf{k}_{zz} \end{bmatrix} \mathbf{d}_e, \tag{15}$$

where \mathbf{K}_e is the element stiffness matrix with the submatrices determined by

$$\begin{aligned} \mathbf{k}_{mm} &= \int_{\Omega_e} \mathbf{B}_m^T \mathbf{D}_1 \mathbf{B}_m d\Omega, \\ \mathbf{k}_{bb} &= \int_{\Omega_e} z^2 \mathbf{C}_b^T \mathbf{D}_1 \mathbf{C}_b d\Omega, \\ \mathbf{k}_{ss} &= \int_{\Omega_e} f^2 \mathbf{C}_s^T \mathbf{D}_1 \mathbf{C}_s d\Omega + \int_{\Omega_e} g^2 \mathbf{B}_s^T \mathbf{D}_2 \mathbf{B}_s d\Omega, \\ \mathbf{k}_{zz} &= \int_{\Omega_e} g^2 \mathbf{B}_z^T \mathbf{D}_1 \mathbf{B}_z d\Omega + \int_{\Omega_e} g^2 \mathbf{B}_{s2}^T \mathbf{D}_2 \mathbf{B}_{s2} d\Omega, \\ \mathbf{k}_{mb} &= \int_{\Omega_e} z \mathbf{B}_m^T \mathbf{D}_1 \mathbf{C}_b d\Omega, \end{aligned}$$

$$\begin{aligned} \mathbf{k}_{\text{ms}} &= \int_{\Omega_e} f \mathbf{B}_m^T \mathbf{D}_1 \mathbf{C}_s d\Omega, \\ \mathbf{k}_{\text{bs}} &= \int_{\Omega_e} z f \mathbf{C}_b^T \mathbf{D}_1 \mathbf{C}_s d\Omega, \\ \mathbf{k}_{\text{bz}} &= \int_{\Omega_e} z g_z \mathbf{C}_b^T \mathbf{D}_1 \mathbf{B}_z d\Omega, \\ \mathbf{k}_{\text{sz}} &= \int_{\Omega_e} f g_z \mathbf{C}_s^T \mathbf{D}_1 \mathbf{B}_z d\Omega + \int_{\Omega_e} g^2 \mathbf{B}_{s1}^T \mathbf{D}_2 \mathbf{B}_{s2} d\Omega. \end{aligned} \quad (16)$$

Substituting Eq. (11) into Eq. (8), the work done by the external force acting on the element is:

$$W_e = \int_{\Omega_e} (w_b + w_s + w_z) q(x, y) d\Omega = \mathbf{F}_e \mathbf{d}_e, \quad (17)$$

in which, $\mathbf{F}_e = \int_{\Omega} \mathbf{N}_w^T q(x, y) d\Omega$ is the node load vector and $\mathbf{N}_w = [\mathbf{0} \quad \mathbf{0} \quad \mathbf{H} \quad \mathbf{H} \quad \mathbf{N}]$ is the shape function matrix of the displacement w which is determined according to the node displacement of the element.

By using the virtual work principle $\delta \left(\sum_{\text{nel}} U_e - \sum_{\text{nel}} W_e \right) = 0$, the governing equations of the sandwich plate are derived by the following formulation:

$$\mathbf{K}\mathbf{D} = \mathbf{F}, \quad (18)$$

where \mathbf{D} is the global node displacement vector; $\mathbf{K} = \sum_{\text{nel}} \mathbf{K}_e$, $\mathbf{F} = \sum_{\text{nel}} \mathbf{F}_e$ are the global stiffness matrix and the global load vector of the sandwich plate, respectively, and symbol “ nel ” represents the number of discretized elements of the sandwich plate. Note that, \mathbf{K}_e and \mathbf{F}_e are determined by using the Gaussian quadrature integration method with four interpolating points. After imposing the boundary condition and solving Eq. (18), the displacement and strain field can be determined through their relations.

For the finite element analysis, boundary conditions (BCs) are taken according to the geometric constraints at the edges. In this paper, BCs are given as follows.

Clamped support (C):

$u_0 = v_0 = w_b = w_s = w_z = w_{b,x} = w_{b,y} = w_{s,x} = w_{s,y} = 0$ at all edges.

Simple support (S):

$u_0 = w_b = w_s = w_z = w_{b,x} = w_{s,x} = 0$ at $x = 0$ & $x = a$ or $x = a/2$,

$v_0 = w_b = w_s = w_z = w_{b,y} = w_{s,y} = 0$ at $y = 0$ & $y = b$ or $y = b/2$.

Free support (F): all DOFs at the boundary edge are non-zero.

4 Numerical results and discussion

This section aims to perform the numerical examples to illustrate novel contributions including: 1) verification of

the reliability of the proposed method; 2) presentation of new results in the bending displacement and stress of FGP sandwich plates including rectangular and L-shape models.

4.1 Verification examples

Firstly, consider a rectangular FG sandwich plate as shown in Fig. 1. The uniformly distributed load q_0 or the sinusoidal distributed load $q(x, y) = q_0 \sin\left(\frac{\pi x}{a}\right) \sin\left(\frac{\pi y}{b}\right)$ is applied. The material properties are provided in Table 1. The dimensionless parameters are introduced by the following formulations:

For the rectangular sandwich plate:

$$\begin{aligned} w^* &= \frac{10E_0h}{q_0a^2} w\left(\frac{a}{2}, \frac{b}{2}\right), \\ \sigma_x^*(z) &= \frac{10h^2}{q_0a^2} \sigma_x\left(\frac{a}{2}, \frac{b}{2}, z\right), \\ \sigma_z^*(z) &= \frac{10h^2}{q_0a^2} \sigma_z\left(\frac{a}{2}, \frac{b}{2}, z\right), \\ \tau_{xz}^*(z) &= \frac{h}{q_0a} \tau_{xz}\left(0, \frac{b}{2}, z\right), \\ E_0 &= 1 \text{ GPa}. \end{aligned} \quad (19a)$$

For the L-shape sandwich plate:

$$\begin{aligned} w^* &= \frac{10E_0h}{q_0a^2} w\left(\frac{a}{4}, \frac{3b}{4}\right), \\ \sigma_x^*(z) &= \frac{10h^2}{q_0a^2} \sigma_x\left(\frac{a}{4}, \frac{3b}{4}, z\right), \\ \sigma_z^*(z) &= \frac{10h^2}{q_0a^2} \sigma_z\left(\frac{a}{4}, \frac{3b}{4}, z\right), \\ \tau_{xz}^*(z) &= \frac{h}{q_0a} \tau_{xz}\left(a, \frac{3b}{4}, z\right). \end{aligned} \quad (19b)$$

The displacement w^* and stress $\sigma_x^*(z)$ of the completely simply supported square sandwich (SSSS) plate with FGM skins and ceramic core under the action of the sinusoidally distributed force are shown in Table 2. Moreover, some comparison results can be seen in Fig. 4. In these table and figure, numerical results of the present work are compared with published work of Zenkour [40] using third-order shear deformation theory (TSĐT) and with work of Thai et al. [50] employing FSĐT. The thickness of plate is $h = a/10$, the material properties are shown in Table 1 with the ceramic being replaced by ZrO_2 with $E_c = 151 \text{ GPa}$, $v_c = 0.3$. It can be seen that the displacement and stress converge at mesh size 16×16 . Moreover, the obtained results are close to those of TSĐT [40] and better than those of FSĐT [50]. It can be asserted that the results from our work are more reliable

Table 2 The comparison of the dimensionless displacement and stress of SSSS FGP sandwich plates with different mesh sizes

k	scheme	displacement and stress	mesh size					Zenkour [40]	Thai et al. [50]
			12 × 12	14 × 14	16 × 16	18 × 18	20 × 20		
0	2-1-2	w*	0.1983	0.1979	0.1976	0.1976	0.1976	0.1961	0.1961
		$\sigma_x^*(h/2)$	2.0204	2.0136	2.0092	2.0092	2.0092	2.0499	1.9758
	1-1-1	w*	0.1983	0.1979	0.1976	0.1976	0.1976	0.1961	0.1961
		$\sigma_x^*(h/2)$	2.0204	2.0136	2.0092	2.0092	2.0092	2.0499	1.9758
	2-2-1	w*	0.1983	0.1979	0.1976	0.1976	0.1976	0.1961	0.1961
		$\sigma_x^*(h/2)$	2.0204	2.0136	2.0092	2.0092	2.0092	2.0499	1.9758
1	1-2-1	w*	0.1983	0.1979	0.1976	0.1976	0.1976	0.1961	0.1961
		$\sigma_x^*(h/2)$	2.0204	2.0136	2.0092	2.0092	2.0092	2.0499	1.9758
	2-1-2	w*	0.3097	0.3091	0.3087	0.3087	0.3087	0.3063	0.3064
		$\sigma_x^*(h/2)$	1.4808	1.4758	1.4726	1.4726	1.4726	1.4959	1.4517
	1-1-1	w*	0.2952	0.2946	0.2943	0.2943	0.2943	0.2920	0.2920
		$\sigma_x^*(h/2)$	1.4111	1.4063	1.4033	1.4033	1.4033	1.4262	1.3830
2	2-2-1	w*	0.2836	0.283	0.2827	0.2827	0.2827	0.2809	0.2809
		$\sigma_x^*(h/2)$	1.3027	1.2983	1.2954	1.2954	1.2954	1.3206	1.2775
	1-2-1	w*	0.2739	0.2734	0.2730	0.2730	0.2730	0.2709	0.2710
		$\sigma_x^*(h/2)$	1.3076	1.3033	1.3004	1.3004	1.3004	1.3231	1.2810
	1-1-1	w*	0.3562	0.3555	0.3551	0.3551	0.3551	0.3523	0.3526
		$\sigma_x^*(h/2)$	1.7070	1.7013	1.6976	1.6976	1.6976	1.7214	1.6750
10	2-1-2	w*	0.4086	0.4078	0.4073	0.4073	0.4073	0.4041	0.3894
		$\sigma_x^*(h/2)$	1.9573	1.9508	1.9465	1.9465	1.9465	1.9713	1.9216
	1-1-1	w*	0.3898	0.3890	0.3886	0.3886	0.3886	0.3855	0.3724
		$\sigma_x^*(h/2)$	1.8710	1.8647	1.8606	1.8606	1.8606	1.8838	1.8375
	2-2-1	w*	0.3648	0.3641	0.3637	0.3637	0.3637	0.3622	0.3492
		$\sigma_x^*(h/2)$	1.6450	1.6393	1.6357	1.6357	1.6357	1.6666	1.6160
	1-2-1	w*	0.3520	0.3514	0.3509	0.3509	0.3509	0.3482	0.3361
		$\sigma_x^*(h/2)$	1.6899	1.6843	1.6806	1.6806	1.6806	1.7042	1.6587

$$\text{Note: } \text{Er}(\%) = 100 \times \frac{|\text{Present} - \text{Reference}|}{\text{Reference}}.$$

than those of Thai et al. [50] because the FSDT has omitted the higher-order displacement components. The computed results are in good agreement with those of other published, specifically, less than 1% for the

displacement and are less than 1.8% for the stress. So, it can be confirmed that the current formula guarantees accuracy and reliability. From here, the mesh size 16×16 is used for the next examples.

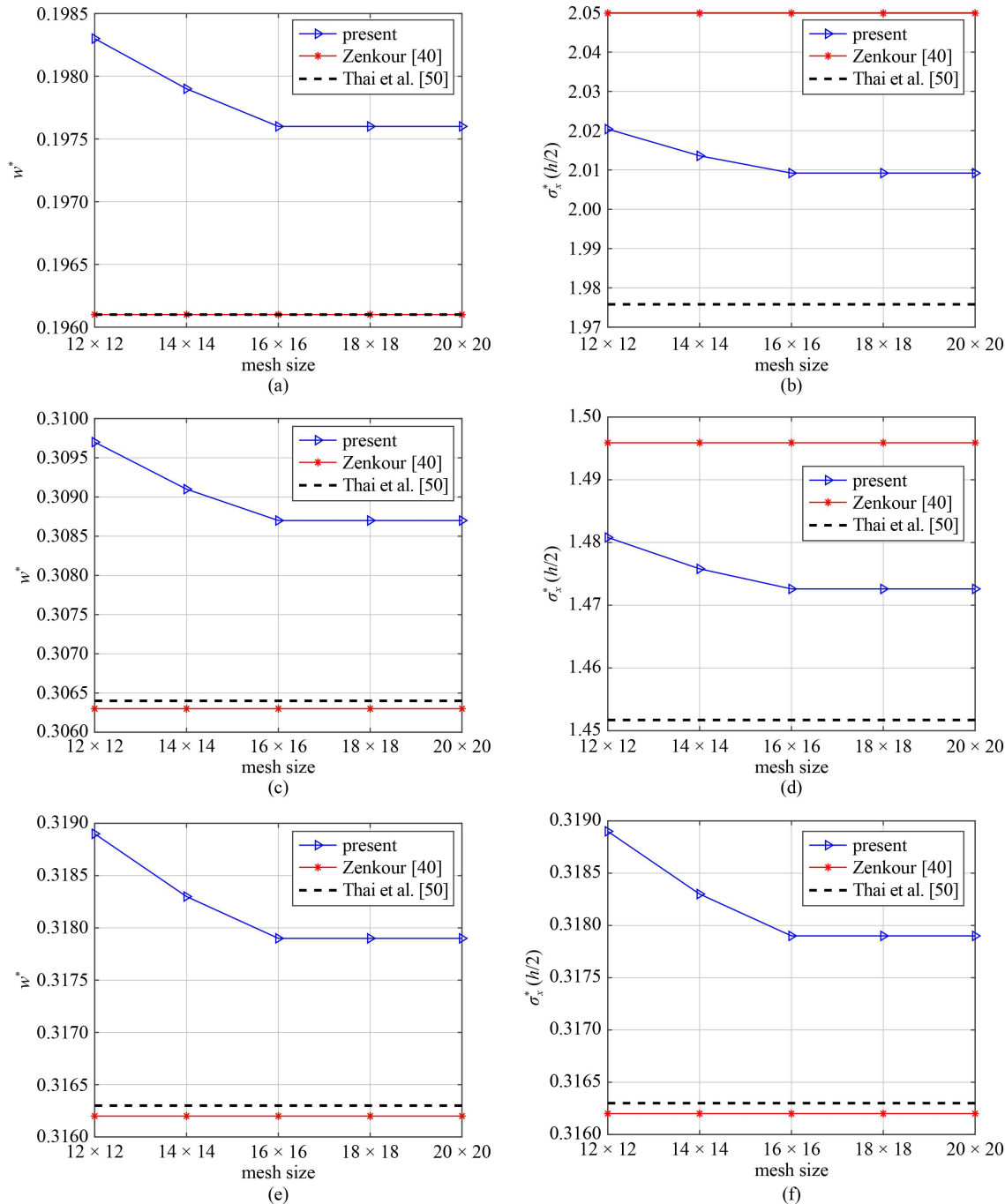
Next, to ensure the performance of the proposed element, we compare the displacement and stress results of the FGM plate with those of Vasiraja and Nagaraj [70] using ANSYS®15.0 software. In that study, they used a Shell181 element with a mesh size 50×50 . The results shown in Tables 3 and 4 once again confirm the reliability and accuracy of the present element.

Finally, the ability to overcome shear locking of this element for the cases of FGM ($\text{Al}_2\text{O}_3/\text{Al}$) square plates with different BCs is demonstrated in Fig. 5. It is observed that the dimensionless deflection of the center-point of FGM plates is almost independent of the change

of the length-to-thickness ratio $\frac{a}{h}$ when the plates become very thin. It can be concluded that the shear locking problem is corrected for the plates with four BCs, and also for five different power-law indexes, $k = 0, 0.5, 1, 2, 4$.

4.2 The rectangular functionally graded porous sandwich plate

Firstly, the effect of power-law index k on the static response of square FGP sandwich plates is studied. Figure 6 and Table 5 show displacement and stress of



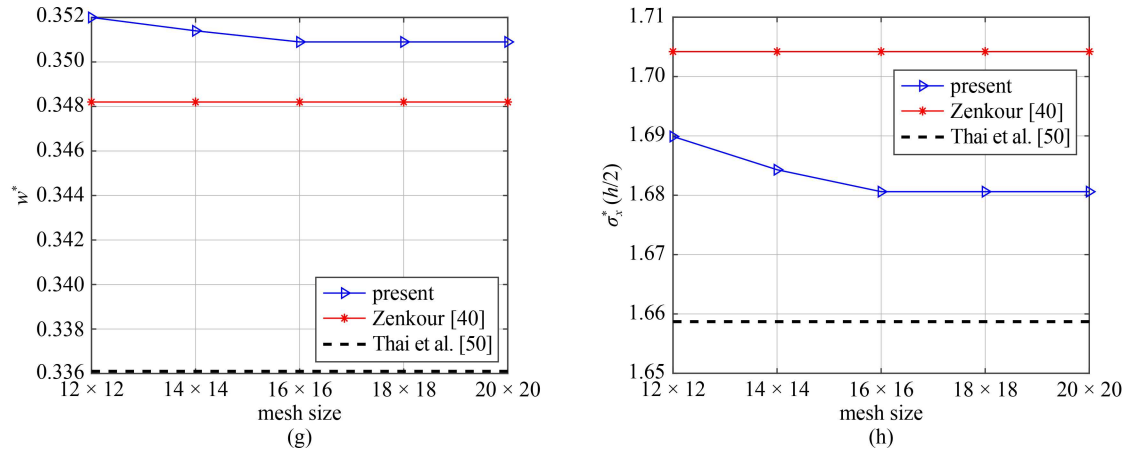


Fig. 4 The displacement and stress of SSSS FGM sandwich plates with different mesh sizes. (a) The comparison of the dimensionless displacement with $k = 0$, scheme 1-1-1; (b) the comparison of the dimensionless stress with $k = 0$, scheme 1-1-1; (c) the comparison of the dimensionless displacement with $k = 1$, scheme 2-1-2; (d) the comparison of the dimensionless stress with $k = 1$, scheme 2-1-2; (e) the comparison of the dimensionless displacement with $k = 2$, scheme 2-2-1; (f) the comparison of the dimensionless stress with $k = 2$, scheme 2-2-1; (g) the comparison of the dimensionless displacement with $k = 10$, scheme 2-2-1; (h) the comparison of the dimensionless stress with $k = 10$, scheme 2-2-1.

Table 3 Dimensionless central displacement \bar{w} , in-plane stress $\bar{\sigma}_x$ and shear stress $\bar{\tau}_{xz}$ of CCCC thin FGM ($\text{Al}_2\text{O}_3/\text{Al}$) square plate ($a/h = 100$) under uniformly distributed load q_0

power law-index	$\bar{w} = \frac{E_c h^3}{12(1-\nu^2)q_0 a^4} w\left(\frac{a}{2}, \frac{b}{2}\right)$		$\bar{\sigma}_x = \frac{h}{q_0 a} \sigma_x\left(\frac{a}{2}, \frac{b}{2}, \frac{h}{2}\right)$		$\bar{\tau}_{xz} = \frac{h}{q_0 a} \tau_{xz}\left(0, \frac{b}{2}, 0\right)$	
	present	Vasiraja Nagaraj [70]	present	Vasiraja Nagaraj [70]	present	Vasiraja Nagaraj [70]
ceramic	0.001244	0.001237	28.3122	28.308	0.639017	0.638044
0.5	0.001883	0.001949	36.6621	36.652	0.665653	0.665576
1	0.002426	0.002540	42.8435	42.822	0.693451	0.692580
2	0.003065	0.003264	48.16327	49.154	0.666412	0.665902
5	0.003644	0.003870	54.4678	54.402	0.603652	0.603208
metal	0.006455	0.006883	28.3114	28.308	0.639017	0.638044

Table 4 Dimensionless central displacement \bar{w} , in-plane stress $\bar{\sigma}_x$ and shear stress $\bar{\tau}_{xz}$ of SSSS thick FGM ($\text{Al}_2\text{O}_3/\text{Al}$) square plate ($a/h = 10$) under uniformly distributed load q_0

power law-index	$\bar{w} = \frac{10E_c h^3}{q_0 a^4} w\left(\frac{a}{2}, \frac{b}{2}\right)$		$\bar{\sigma}_x = \frac{h}{q_0 a} \sigma_x\left(\frac{a}{2}, \frac{b}{2}, \frac{h}{2}\right)$		$\bar{\tau}_{xz} = \frac{h}{q_0 a} \tau_{xz}\left(0, \frac{b}{2}, 0\right)$	
	present	Vasiraja Nagaraj [70]	present	Vasiraja Nagaraj [70]	present	Vasiraja Nagaraj [70]
ceramic	0.4702	0.466	2.9075	2.872	0.5020	0.491
0.5	0.7048	0.712	3.7887	3.719	0.5119	0.501
1	0.9009	0.927	4.4909	4.345	0.5028	0.491
2	1.1344	1.193	5.2529	4.988	0.4657	0.466
5	1.3751	1.444	6.1746	5.521	0.4083	0.427
metal	2.4443	2.530	2.9075	2.872	0.4992	0.491

SSSS square FGP sandwich plate (scheme 1-2-1) with the thickness $a/h = 25$ (a is fixed), and with the porosity coefficient $\xi = 0.1$. [Figure 7](#) and [Table 6](#) illustrate displacement and stress of SCSC square FGP sandwich

plate (scheme 1-1-1) with the thickness $a/h = 30$ and with the porosity coefficient $\xi = 0.15$. These figure and table show that increase in power-law index k leads to increase of the displacement and stress of FGP sandwich plates.

This is as expected because the increase of the power-law index k results in increasing the volume of metal in the structure and thus it reduces the stiffness of FGP sandwich plates.

Secondly, Fig. 8 and Table 7 show displacement and stress response of fully clamped (CCCC) square FGP sandwich plates (scheme 1-1-1) with the thickness $a/h = 15$ versus porosity coefficient ξ with power-law index $k = 1$. It can be observed that the increase of the porosity coefficient ξ results in the increase of the

$a/h = 50$ versus porosity coefficient ξ with power-law index $k = 2$. In addition, Fig. 9 and Table 8 present displacement and stress response of SFSF square FGP sandwich plates (scheme 1-4-1) with the thickness $a/h = 15$ versus porosity coefficient ξ with power-law index $k = 1$. It can be observed that the increase of the porosity coefficient ξ results in the increase of the

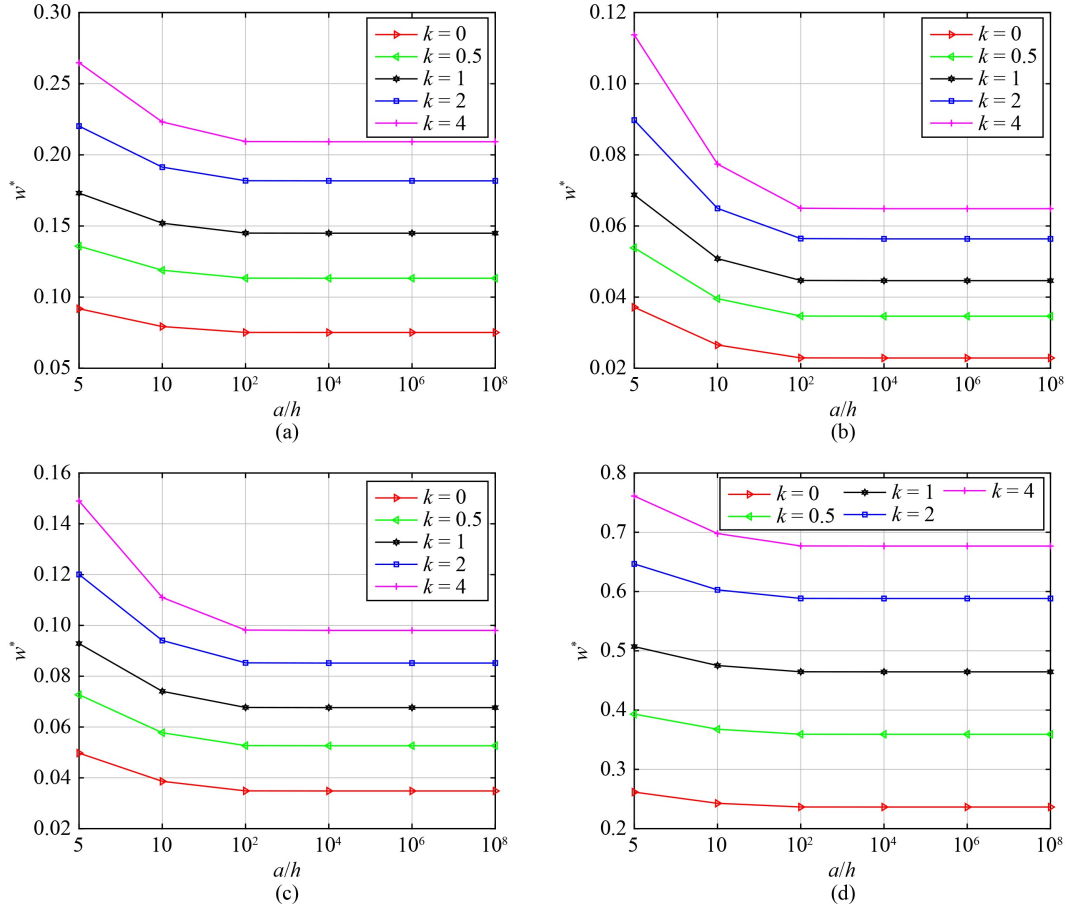
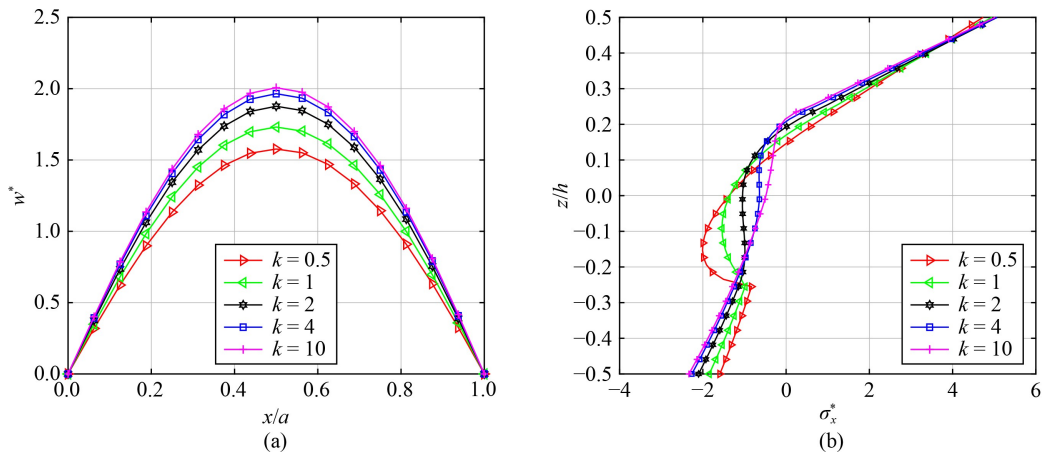


Fig. 5 Dimensionless deflection of the center-point of FGM plates ($w^* = w_c \frac{100E_m h^3}{12q_0(1-\nu^2)a^4}$) subjected to a uniform load. (a) The SSSS FGM plates; (b) the CCCC FGM plates; (c) the SCSC FGM plates; (d) the SFSS FGM plates.



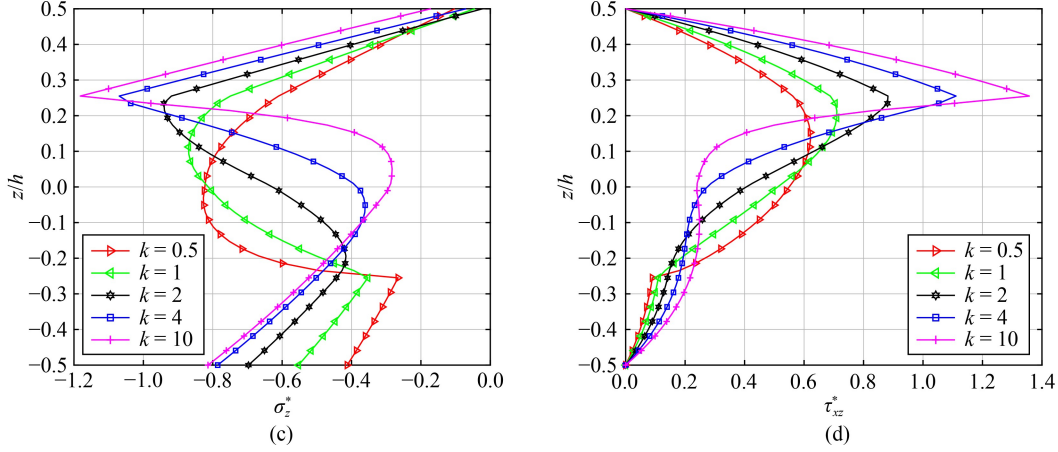


Fig. 6 The static response of SSSS FGP sandwich plates (scheme 1-2-1) versus power-law index k . (a) The displacement of the midline of FGP sandwich plates; (b) the stress $\sigma_x^*(z)$ of the center-point of FGP sandwich plates through the thickness; (c) the stress $\sigma_z^*(z)$ of the center-point of FGP sandwich plates through the thickness; (d) the stress $\tau_{xz}^*(z)$ of the C-point of FGP sandwich plates through the thickness.

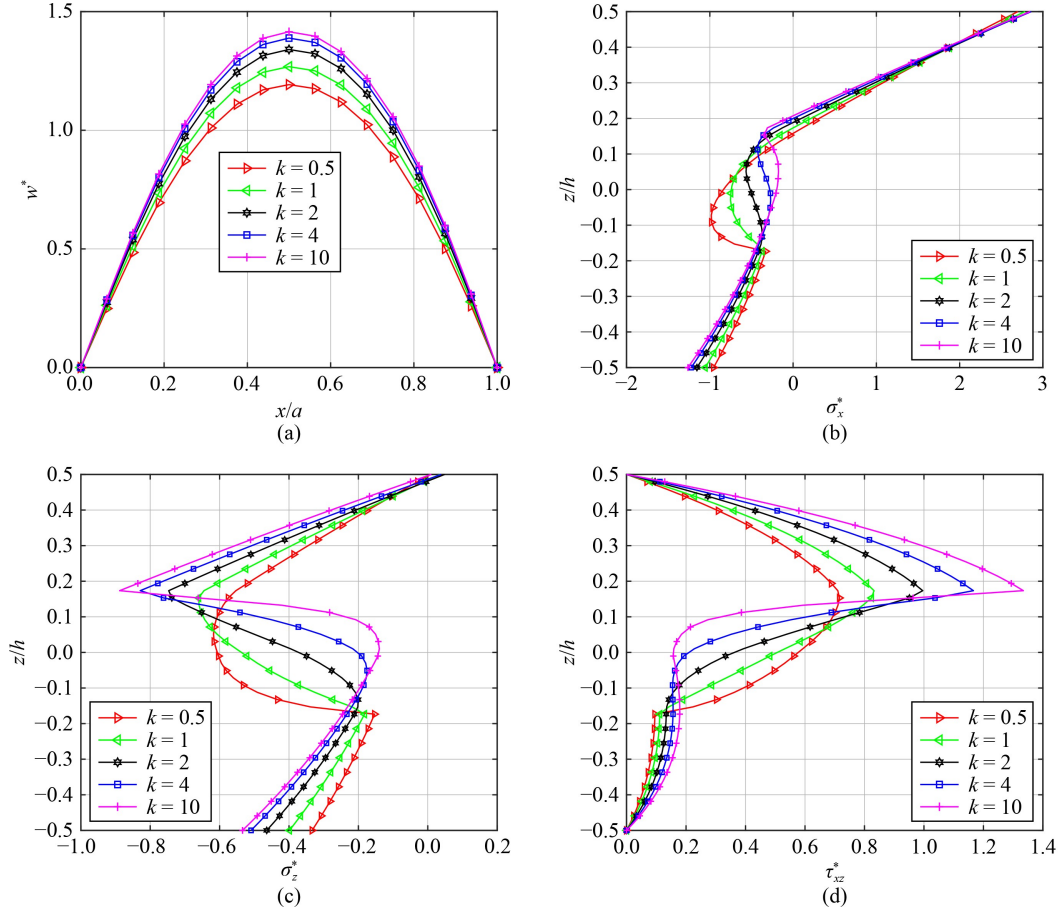


Fig. 7 The static response of SCSC FGP sandwich plates (scheme 1-1-1) versus power-law index k . (a) The displacement of the midline of FGP sandwich plates; (b) the stress $\sigma_x^*(z)$ of the center-point of FGP sandwich plates through the thickness; (c) the stress $\sigma_z^*(z)$ of the center-point of FGP sandwich plates through the thickness; (d) the stress $\tau_{xz}^*(z)$ of the C-point of FGP sandwich plates through the thickness.

displacement and stress response of FGP sandwich plates. This is reasonable since the increase in volume makes reduce the stiffness of FGP sandwich plates.

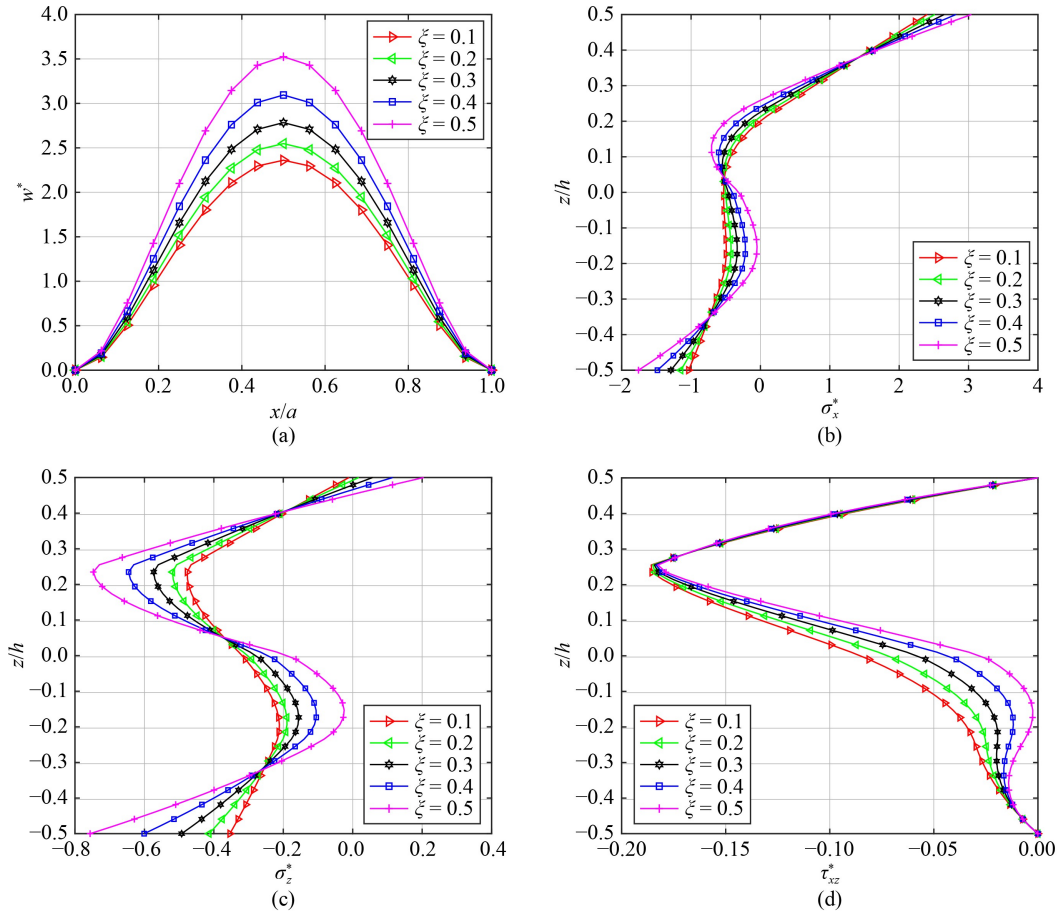
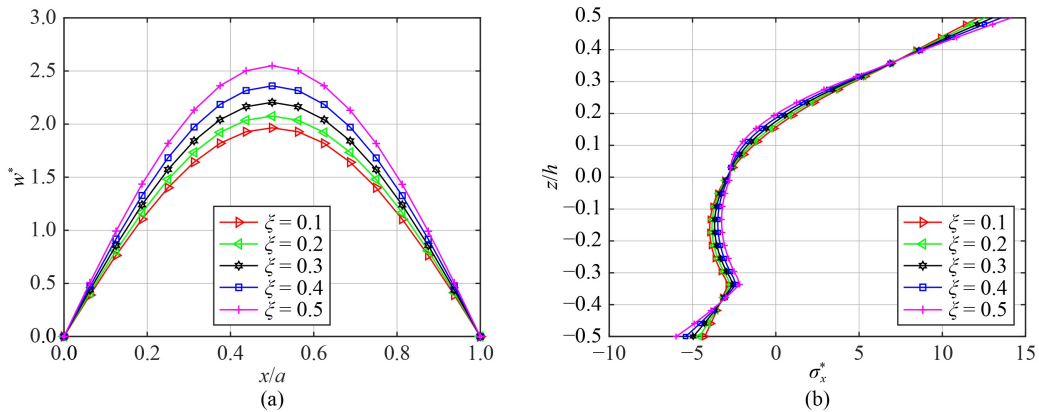
Next, the effect of the thickness ratio between layers (schemes) on the static response of FGP sandwich plates are plotted in Figs. 10 and 11 and provided in Tables 9

Table 5 The displacement and stress of SSSS FGP sandwich plates versus power-law index k (scheme 1-2-1)

parameters	$k = 0.5$	$k = 1$	$k = 2$	$k = 4$	$k = 10$
max (w^*)	1.5769	1.7310	1.8768	1.9648	2.0067
$\sigma_x^*(h/2)$	4.7358	4.9465	5.0721	5.0709	5.0223
$\sigma_z^*(h/2)$	-0.1026	-0.0448	-0.0221	-0.0698	-0.1711
$\tau_{xz}^*(0)$	0.5491	0.5105	0.4040	0.2722	0.2378

Table 6 The displacement and stress of SCSC FGP sandwich plates versus power-law index k (scheme 1-1-1)

parameters	$k = 0.5$	$k = 1$	$k = 2$	$k = 4$	$k = 10$
max (w^*)	1.1924	1.2681	1.3406	1.3885	1.4152
$\sigma_x^*(h/2)$	2.6989	2.7840	2.8436	2.8592	2.8451
$\sigma_z^*(h/2)$	0.0083	0.0353	0.0483	0.0385	0.0103
$\tau_{xz}^*(0)$	0.5763	0.5054	0.3598	0.206	0.1549

**Fig. 8** The static response of CCCC FGP sandwich plates (scheme 1-1-1) versus porosity coefficient ξ . (a) The displacement of the midline of FGP sandwich plates; (b) the stress $\sigma_x^*(z)$ of the center-point of FGP sandwich plates through the thickness; (c) the stress $\sigma_z^*(z)$ of the center-point of FGP sandwich plates through the thickness; (d) the stress $\tau_{xz}^*(z)$ of the C-point of the FGP sandwich plate through the thickness.

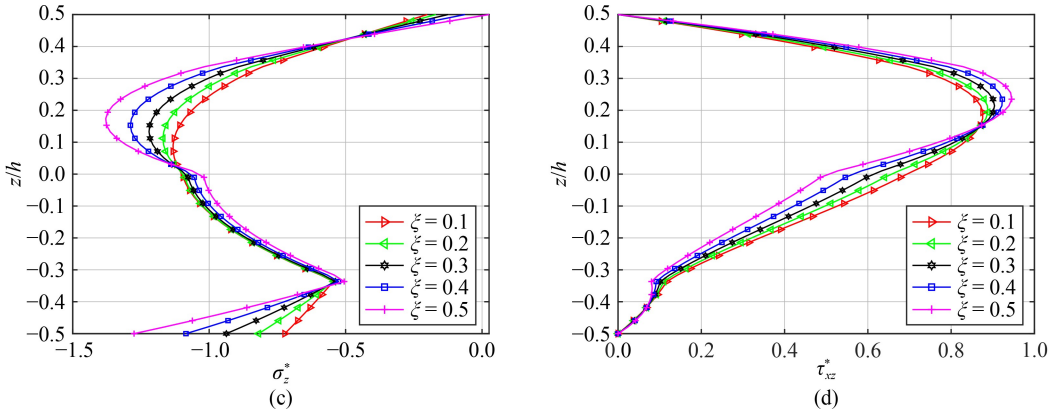


Fig. 9 The static response of SFSF FGP sandwich plates (scheme 1-4-1) versus porosity coefficient ξ . (a) The displacement of the midline of FGP sandwich plates; (b) the stress $\sigma_x^*(z)$ of the center-point of FGP sandwich plates through the thickness; (c) the stress $\sigma_z^*(z)$ of the center-point of FGP sandwich plates through the thickness; (d) the stress $\tau_{xz}^*(z)$ of the C-point of the FGP sandwich plate through the thickness.

Table 7 The displacement and stress of CCCC FGP sandwich plates versus porosity coefficient ξ (scheme 1-1-1)

parameters	$\xi = 0.1$	$\xi = 0.2$	$\xi = 0.3$	$\xi = 0.4$	$\xi = 0.5$
w^*	2.3609	2.5479	2.7840	3.0943	3.5251
$\sigma_x^*(h/2)$	2.4028	2.5142	2.6486	2.8175	3.0417
$\sigma_z^*(h/2)$	-0.0106	0.0174	0.0573	0.1155	0.2046
$\tau_{xz}^*(0)$	-0.0851	-0.0716	-0.0575	-0.0425	-0.0266

Table 8 The displacement and stress of SFSF FGP sandwich plates versus porosity coefficient ξ (scheme 1-4-1)

parameters	$\xi = 0.1$	$\xi = 0.2$	$\xi = 0.3$	$\xi = 0.4$	$\xi = 0.5$
w^*	2.2870	2.4194	2.5749	2.7611	2.9897
$\sigma_x^*(h/2)$	12.1422	12.5523	13.0116	13.5344	14.1424
$\sigma_z^*(h/2)$	-0.2010	-0.1692	-0.1247	-0.0624	0.0257
$\tau_{xz}^*(0)$	0.6928	0.6543	0.6099	0.5580	0.4970

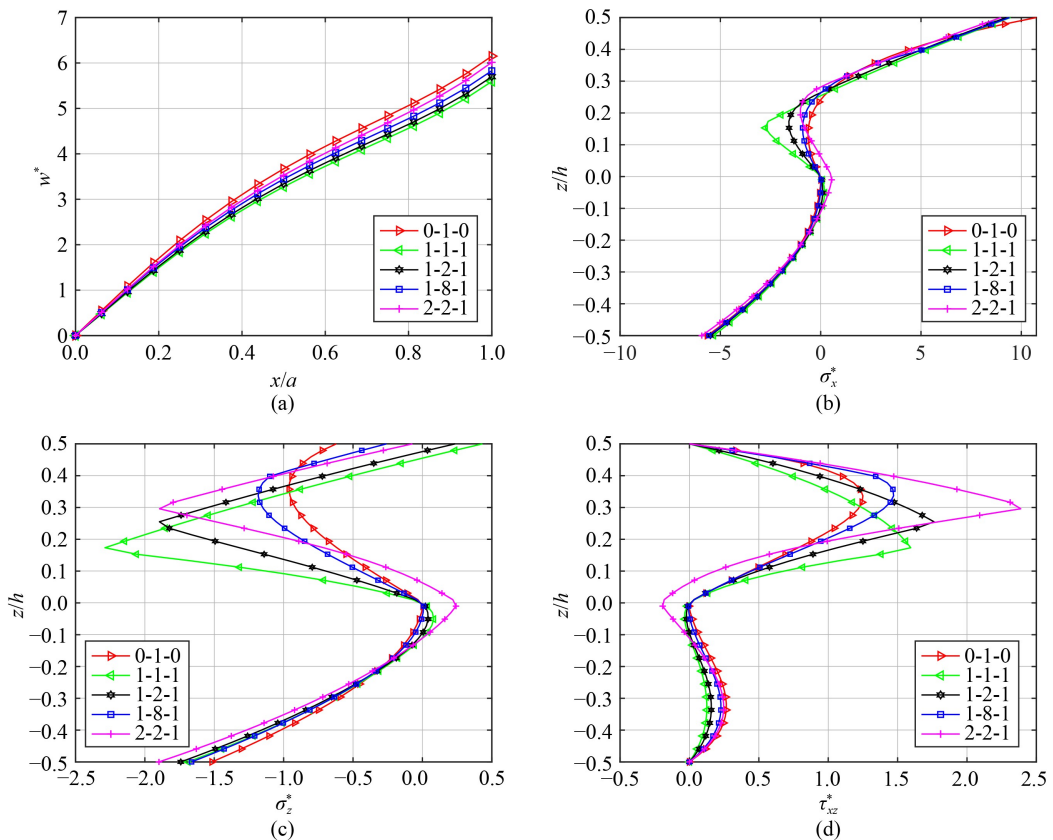


Fig. 10 The static response of SSFS FGP sandwich plates versus different schemes. (a) The displacement of the midline of FGP sandwich plates; (b) the stress $\sigma_x^*(z)$ of the center-point of FGP sandwich plates through the thickness; (c) the stress $\sigma_z^*(z)$ of the center-point of FGP sandwich plates through the thickness; (d) the stress $\tau_{xz}^*(z)$ of the C-point of the FGP sandwich plate through the thickness.

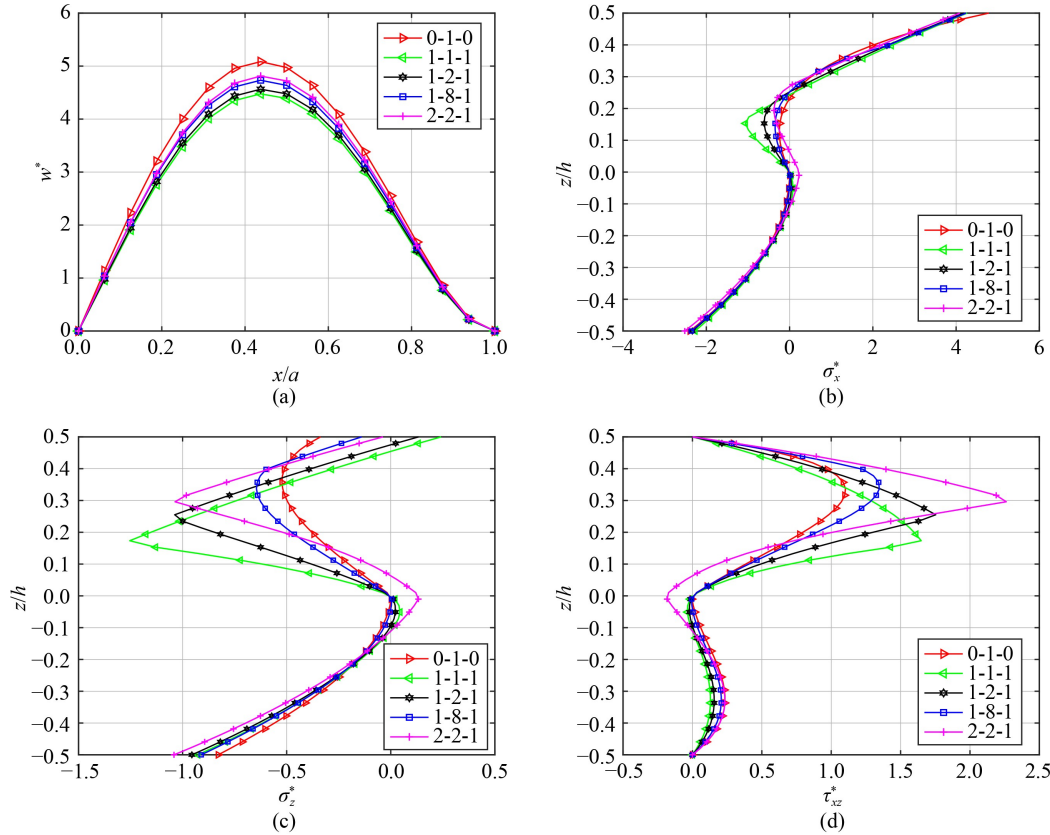


Fig. 11 The static response of SSCS FGP sandwich plates versus different schemes. (a) The displacement of the midline of FGP sandwich plates; (b) the stress $\sigma_x^*(z)$ of the center-point of FGP sandwich plates through the thickness; (c) the stress $\sigma_z^*(z)$ of the center-point of FGP sandwich plates through the thickness; (d) the stress $\tau_{xz}^*(z)$ of the C-point of FGP sandwich plates through the thickness.

Table 9 The displacement and stress of SSSS FGP sandwich plates versus schemes

parameters	value				
	0-1-0	1-1-1	1-2-1	1-8-1	2-2-1
w^*	6.1509	5.5924	5.6977	5.8287	6.0131
$\sigma_x^*(h/2)$	10.7513	9.4641	9.2555	9.4142	8.9882
$\sigma_z^*(h/2)$	-0.6205	0.4326	0.2359	-0.2589	-0.072
$\tau_{xz}^*(0)$	-0.0074	-0.0035	-0.0044	-0.0064	-0.2087

and 10 with porosity coefficient $\xi = 0.4$ and power-law index $k = 4$. Specifically, Fig. 10 and Table 9 present the displacement and stress response of SSFS FGP sandwich plates with the thickness $a/h = 20$ while Fig. 11 and Table 10 show the static response of SSCS FGP sandwich plates with the thickness $a/h = 40$. From these figures and tables, it can be found that when the FGP sandwich plate thickness is constant, the thickness ratio between layers significantly affects the static bending of FGP sandwich plates. Observing the graphs, we can see that the scheme 1-1-1 gives the smallest displacement and stress response, whereas the scheme 0-1-0 (the isotropic FGP plate) gives the largest displacement and stress response. This confirms that the FGP core has a positive effect on the static response of sandwich plates and is more efficient

Table 10 The displacement and stress of CCCC FGP sandwich plates versus schemes

parameters	scheme				
	0-1-0	1-1-1	1-2-1	1-8-1	2-2-1
w^*	5.0841	4.4759	4.5641	4.7329	4.8117
$\sigma_x^*(h/2)$	4.7835	4.2647	4.1825	4.2377	4.0886
$\sigma_z^*(h/2)$	-0.3376	0.2420	0.1333	-0.1398	-0.0373
$\tau_{xz}^*(0)$	-0.0065	-0.0036	-0.0044	-0.0058	-0.1977

than the isotropic FGP plates. Herein, C-point has coordinates $(0, \frac{b}{2}, z)$.

Besides, Table 11 provides more displacement and stress results of SSSS FGP sandwich plates versus power-law index k corresponding to specific values of a/h ratios and schemes while Table 12 presents the displacement and stress results of CCCC FGP sandwich plates versus porosity coefficient ξ . Note that, the order of BCs is denoted sequentially from edge 1 to edge 4.

4.3 The L-shape functionally graded porous sandwich plate

This part investigates the static bending of FGP L-shape

Table 11 Displacement and stress of SSSS FGP sandwich plates versus power-law index k ($\xi = 0.5$)

$\frac{a}{h}$	scheme	w^*				$\sigma_x^*(h/2)$			
		$k = 0.5$	$k = 1.5$	$k = 4.5$	$k = 10.5$	$k = 0.5$	$k = 1.5$	$k = 4.5$	$k = 10.5$
15	2-1-2	0.8784	0.9727	1.0567	1.0909	6.3092	6.5531	6.6895	6.7067
	1-1-1	0.8068	0.9597	1.1057	1.1628	5.9845	6.4243	6.615	6.5761
	2-2-1	0.9338	1.1028	1.2584	1.3349	6.3485	6.4606	6.194	6.0005
	1-8-1	0.5541	0.8466	1.2147	1.4443	4.6512	5.8802	6.3579	6.2968
25	2-1-2	2.4161	2.6738	2.9015	2.9934	6.3056	6.5505	6.6869	6.7034
	1-1-1	2.2182	2.6359	3.0298	3.1793	5.9786	6.4198	6.609	6.5663
	2-2-1	2.5643	3.0147	3.3936	3.5356	6.343	6.4494	6.1549	5.9230
	1-8-1	1.5180	2.3169	3.2765	3.689	4.6408	5.8674	6.3219	6.1527
45	2-1-2	7.7980	8.6274	9.3581	9.652	6.305	6.5509	6.6881	6.7047
	1-1-1	7.1580	8.5027	9.7641	10.2371	5.9768	6.4193	6.6094	6.5661
	2-2-1	8.2710	9.7063	10.8665	11.2379	6.3419	6.4476	6.1447	5.8988
	1-8-1	4.8916	7.4630	10.4927	11.5449	4.6368	5.8629	6.3109	6.1010
65	2-1-2	16.2553	17.983	19.5043	20.1155	6.3049	6.5511	6.6886	6.7053
	1-1-1	14.9205	17.7219	20.3464	21.3277	5.9764	6.4193	6.6098	6.5665
	2-2-1	17.2388	20.2215	22.6094	23.3412	6.3418	6.4475	6.1431	5.8942
	1-8-1	10.1931	15.5496	21.8323	23.8898	4.6358	5.862	6.3088	6.0899

Table 12 Displacement and stress of CCCC FGP sandwich plates versus porosity coefficient ξ ($k = 2.5$)

$\frac{a}{h}$	scheme	w^*				$\sigma_x^*(h/2)$			
		$k = 0.5$	$k = 2.5$	$k = 5.5$	$k = 9.5$	$k = 0.5$	$k = 2.5$	$k = 5.5$	$k = 9.5$
5	1-1-2	0.0305	0.0325	0.0347	0.0374	2.4846	2.5974	2.7286	2.8848
	1-1-1	0.0373	0.0406	0.0448	0.0504	2.6051	2.7543	2.9404	3.1836
	2-2-1	0.0444	0.0498	0.0571	0.0678	2.6459	2.8007	3.0011	3.2800
	1-6-1	0.0405	0.0445	0.0496	0.0564	2.6255	2.7572	2.9185	3.1251
30	1-1-2	0.8036	0.8552	0.9168	0.9921	2.4375	2.5461	2.6727	2.8238
	1-1-1	0.9119	0.9948	1.1029	1.2510	2.4950	2.6311	2.8017	3.0271
	2-2-1	0.9554	1.0553	1.1933	1.3994	2.4546	2.5721	2.7213	2.9263
	1-6-1	0.9096	0.9885	1.0912	1.2321	2.4831	2.5921	2.724	2.8919
70	1-1-2	4.3360	4.6143	4.947	5.3542	2.4358	2.5443	2.6707	2.8215
	1-1-1	4.9072	5.3533	5.9353	6.7345	2.4914	2.6270	2.7970	3.0214
	2-2-1	5.1152	5.6463	6.3798	7.4766	2.4492	2.5654	2.7130	2.9153
	1-6-1	4.8788	5.2999	5.8479	6.6002	2.479	2.5873	2.7183	2.8847
95	1-1-2	7.9786	8.4909	9.1032	9.8526	2.4357	2.5441	2.6705	2.8212
	1-1-1	9.0272	9.848	10.9188	12.3892	2.4911	2.6266	2.7965	3.0208
	2-2-1	9.405	10.3807	11.7283	13.7437	2.4486	2.5647	2.7121	2.9141
	1-6-1	8.9720	9.7459	10.7531	12.1361	2.4786	2.5868	2.7177	2.8840

sandwich plates with geometrical parameters as shown in Fig. 12, so as to illustrate the effectiveness of the finite element method compared with the analytical method in analyzing the mechanical behavior of the structures, especially when the geometrical model becomes more complex (un-symmetry).

Firstly, some displacement and stress results of SSSSS FGP L-shape sandwich plates (scheme 1-2-1) with $h/a = 20$; $\xi = 0.3$ versus variations with power-law index k and different mesh sizes are provided in Table 13, which indicates that the numerical results converge at mesh size 16×16 . Then, Fig. 13 presents the

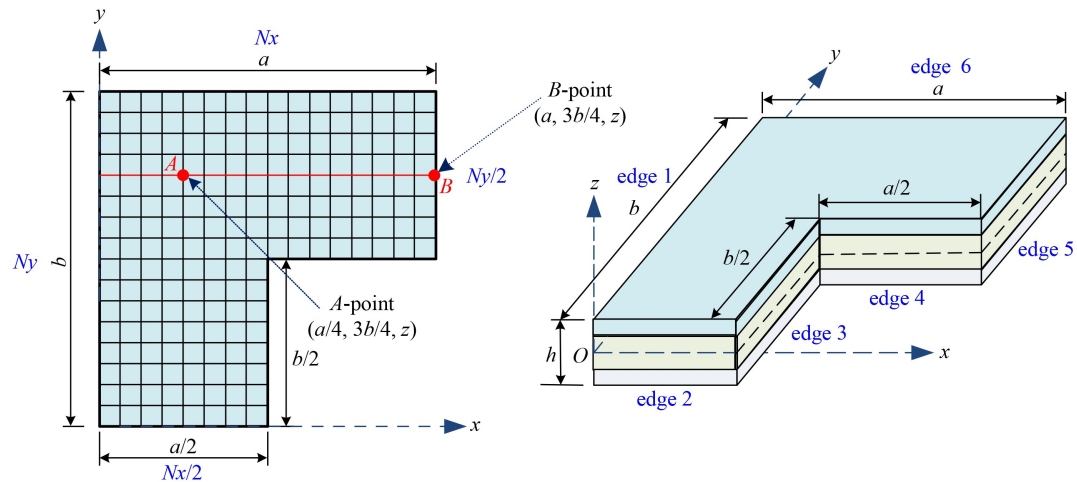


Fig. 12 The schematic diagram for the FGP L-shape sandwich plate and the mesh model.

Table 13 Variations of displacement and stress of SSSSSS FGP L-shape sandwich plates versus with power-law index k (scheme 1-2-1; $h/a = 20$; $\xi = 0.3$)

power law-index	displacement and stress	value				
		12×12	14×14	16×16	18×18	20×20
$k = 0.5$	w^*	0.1563	0.1559	0.1556	0.1556	0.1556
	$\sigma_x^*(h/2)$	1.5970	1.5965	1.5962	1.5962	1.5962
	$\sigma_z^*(h/2)$	-0.0161	-0.0157	-0.0154	-0.0154	-0.0154
	$\tau_{xz}^*(0)$	-0.3376	-0.3371	-0.3367	-0.3367	-0.3367
$k = 1$	w^*	0.1769	0.1765	0.1763	0.1763	0.1763
	$\sigma_x^*(h/2)$	1.6900	1.6906	1.6901	1.6900	1.6900
	$\sigma_z^*(h/2)$	0.0183	0.0180	0.0178	0.0177	0.0177
	$\tau_{xz}^*(0)$	-0.2857	-0.2853	-0.2850	-0.2849	-0.2849
$k = 2$	w^*	0.1990	0.1990	0.1991	0.1990	0.1990
	$\sigma_x^*(h/2)$	1.7621	1.7617	1.7614	1.7613	1.7613
	$\sigma_z^*(h/2)$	0.0432	0.0428	0.0424	0.0424	0.0424
	$\tau_{xz}^*(0)$	-0.1859	-0.1855	-0.1851	-0.1850	-0.1850
$k = 5$	w^*	0.2201	0.2199	0.2197	0.2196	0.2196
	$\sigma_x^*(h/2)$	1.7743	1.7739	1.7735	1.7735	1.7735
	$\sigma_z^*(h/2)$	0.0289	0.0285	0.0281	0.0280	0.0280
	$\tau_{xz}^*(0)$	-0.0420	-0.0416	-0.0412	-0.0411	-0.0411
$k = 10$	w^*	0.2275	0.2270	0.2268	0.2267	0.2267
	$\sigma_x^*(h/2)$	1.7586	1.7581	1.7576	1.7576	1.7576
	$\sigma_z^*(h/2)$	-0.0021	-0.0015	-0.0011	-0.0010	-0.0010
	$\tau_{xz}^*(0)$	-0.0128	-0.0123	-0.0120	-0.0119	-0.0119

displacement and stress response of SSSSSS FGP L-shape sandwich plates, and illustrates that the maximum displacement of FGP L-shape sandwich plates shifts to the left and the elastic line is no longer as symmetric as in the case of rectangular sandwich plates. This is due to the asymmetry of L-shape sandwich plates.

Similarly, the displacement and stress response of CCCCCC FGP L-shape sandwich plates (scheme 1-4-1) with $a/h = 40$, $k = 10$ versus porosity coefficient ξ and different mesh sizes are listed in Table 14, which confirms that the obtained results also converge at a mesh

size 16×16 . Next, the displacement and stress response of CCCCCC FGP L-shape sandwich plates is plotted in Fig. 14. Note that, A-point has coordinates $\left(\frac{a}{4}, \frac{3a}{4}, z\right)$, B-point has coordinates $\left(a, \frac{3a}{4}, z\right)$ and AB-line has the equation as $y = \frac{3a}{4}$ (see Fig. 12), the order of BCs is denoted sequentially from edge 1 to edge 6 and mesh size $N_x \times N_y$ with N_x, N_y are respectively the number of elements divided along the x - and y -axis.

Furthermore, Table 15 and Table 16 present some new

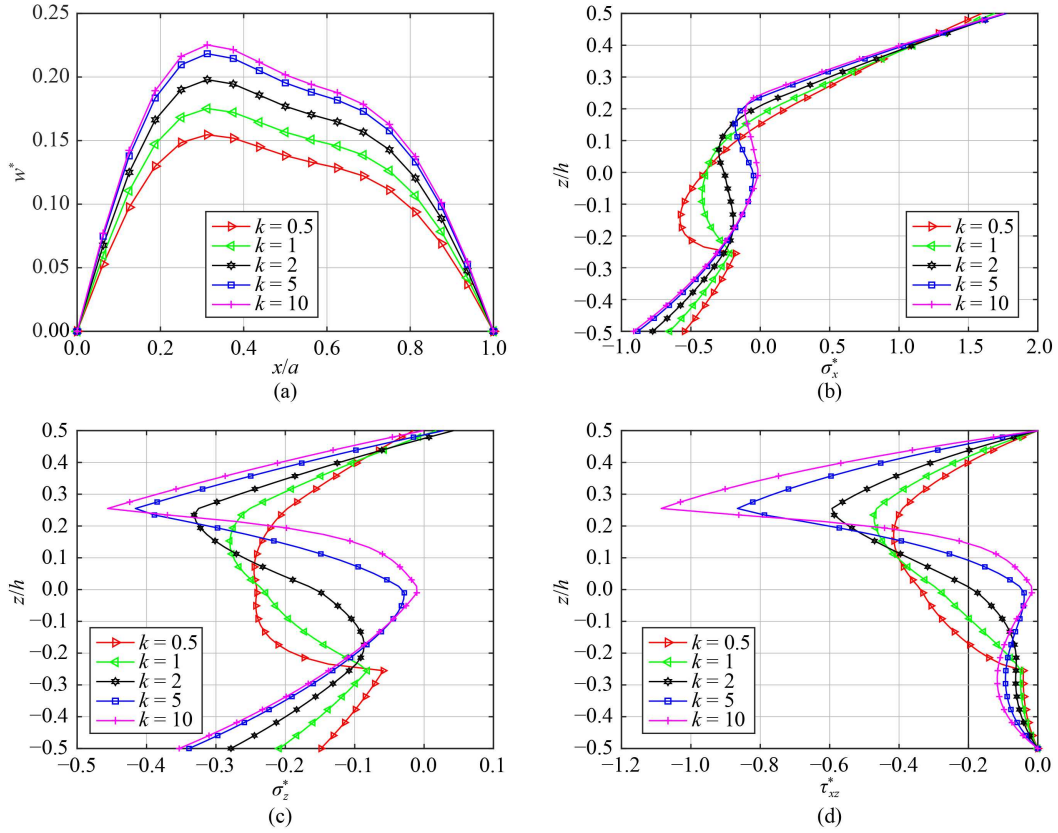


Fig. 13 The static response of SSSSS FGP L-shape sandwich plates (scheme 1-2-1; $h/a = 20$; $\xi = 0.3$). (a) The displacement of the A-y-line of FGP sandwich plates; (b) the stress $\sigma_x^*(z)$ of the A-point of FGP sandwich plates through the thickness; (c) the stress $\sigma_z^*(z)$ of the A-point of FGP sandwich plates through the thickness; (d) the stress $\tau_{xz}^*(z)$ of the B-point of FGP sandwich plates through the thickness.

Table 14 Variations of displacement and stress of CCCCCC FGP L-shape sandwich plates versus with porosity coefficient ξ (scheme 1-4-1; $h/a = 40$; $k = 10$)

porosity coefficient	displacement and stress	value				
		12 × 12	14 × 14	16 × 16	18 × 18	20 × 20
$\xi = 0.05$	w^*	0.2876	0.2870	0.2865	0.2864	0.2864
	$\sigma_x^*(h/2)$	0.7686	0.7680	0.7675	0.7674	0.7674
	$\sigma_z^*(h/2)$	-0.0397	-0.0392	-0.0389	-0.0388	-0.0388
	$\tau_{xz}^*(0)$	0.0128	0.0122	0.0118	0.0117	0.0117
$\xi = 0.15$	w^*	0.3130	0.3126	0.3121	0.3121	0.3121
	$\sigma_x^*(h/2)$	0.7991	0.7987	0.7983	0.7982	0.7982
	$\sigma_z^*(h/2)$	-0.0350	-0.0345	-0.0342	-0.0341	-0.0341
	$\tau_{xz}^*(0)$	0.0084	0.0079	0.0076	0.0075	0.0075
$\xi = 0.25$	w^*	0.3470	0.3466	0.3461	0.3460	0.3460
	$\sigma_x^*(h/2)$	0.8365	0.8360	0.8355	0.8354	0.8354
	$\sigma_z^*(h/2)$	-0.0272	-0.0267	-0.0263	-0.0263	-0.0263
	$\tau_{xz}^*(0)$	0.3471	0.3465	0.3461	0.3460	0.3460
$\xi = 0.35$	w^*	0.3945	0.3940	0.3936	0.3935	0.3935
	$\sigma_x^*(h/2)$	0.8837	0.8832	0.8827	0.8827	0.8827
	$\sigma_z^*(h/2)$	-0.0141	-0.0137	-0.0133	-0.0132	-0.0132
	$\tau_{xz}^*(0)$	-0.0029	-0.0024	-0.0019	-0.0018	-0.0018
$\xi = 0.45$	w^*	0.4673	0.4668	0.4664	0.4663	0.4663
	$\sigma_x^*(h/2)$	0.9493	0.9489	0.9485	0.9485	0.9485
	$\sigma_z^*(h/2)$	0.0114	0.0107	0.0101	0.0100	0.0100
	$\tau_{xz}^*(0)$	-0.0080	-0.0073	-0.0069	-0.0068	-0.0068

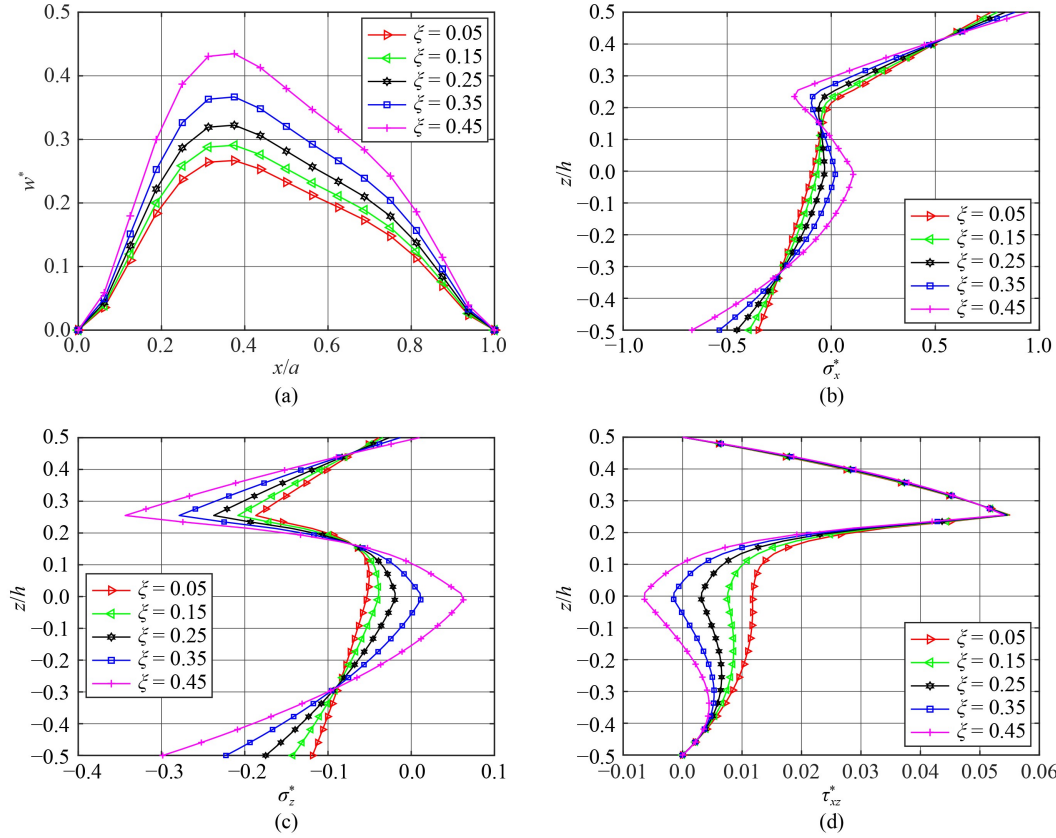


Fig. 14 The static response of CCCCCC FGP L-shape sandwich plates (scheme 1-4-1; $h/a = 40$; $k = 10$). (a) The displacement of the A-y line of FGP sandwich plates; (b) the stress $\sigma_x^*(z)$ of the A-point of FGP sandwich plates through the thickness; (c) the stress $\sigma_z^*(z)$ of the A-point of FGP sandwich plates through the thickness; (d) the stress $\tau_{xz}^*(z)$ of the B-point of FGP sandwich plates through the thickness.

Table 15 Displacement and stress of SSSSSS FGP sandwich plates versus with different parameters ($\xi = 0.45$)

$\frac{a}{h}$	scheme	w^*				$\sigma_x^*(h/2)$			
		$k = 0.5$	$k = 1.5$	$k = 5.5$	$k = 8.5$	$k = 0.5$	$k = 1.5$	$k = 5.5$	$k = 8.5$
15	2-1-2	0.1198	0.1323	0.1448	0.1472	1.9343	2.0125	2.0664	2.0719
	1-1-1	0.1104	0.1308	0.1528	0.1568	1.8389	1.9771	2.0566	2.0576
	2-2-1	0.1275	0.1507	0.179	0.1867	1.9545	2.0177	1.9894	1.9789
	1-8-1	0.0774	0.1172	0.1789	0.2003	1.4551	1.8269	2.0487	2.0761
25	2-1-2	0.3216	0.3542	0.3860	0.3918	1.9076	1.9744	2.0157	2.0187
	1-1-1	0.2962	0.3495	0.4040	0.4133	1.8193	1.9404	1.9979	1.9947
	2-2-1	0.3404	0.3965	0.4501	0.4608	1.9218	1.9632	1.9058	1.8871
	1-8-1	0.2054	0.3097	0.4466	0.4772	1.4480	1.8032	1.9732	1.9803
55	2-1-2	1.5322	1.6856	1.8328	1.8589	1.8937	1.9538	1.9872	1.9886
	1-1-1	1.4107	1.6613	1.9112	1.9516	1.8093	1.9206	1.9642	1.9581
	2-2-1	1.6179	1.8705	2.076	2.104	1.9044	1.9325	1.8578	1.8351
	1-8-1	0.9731	1.4646	2.0519	2.1366	1.4450	1.7915	1.9327	1.9309
85	2-1-2	3.6507	4.0154	4.3645	4.4264	1.8915	1.9504	1.9825	1.9836
	1-1-1	3.3611	3.9569	4.5485	4.6434	1.8077	1.9174	1.9585	1.9518
	2-2-1	3.8534	4.4501	4.921	4.9794	1.9016	1.9274	1.8495	1.8261
	1-8-1	2.3166	3.4856	4.861	5.0403	1.4445	1.7896	1.9259	1.9227

results on the static response of FGP L-shape sandwich plates with variation of the geometrical and material

parameters.

Finally, the variation of deformation field of FGP L-

shape sandwich plates versus with different BCs is shown visually in Fig. 15. It can be concluded that with the same geometry parameters and material properties, the displacement of the CCCCCC L-shape sandwich plate is

Table 16 Displacement and stress of CCCCCC FGP sandwich plates versus with different parameters ($k = 3.5$)

$\frac{a}{h}$	scheme	w^*				$\sigma_x^*(h/2)$			
		$\xi = 0.1$	$\xi = 0.2$	$\xi = 0.3$	$\xi = 0.4$	$\xi = 0.1$	$\xi = 0.2$	$\xi = 0.3$	$\xi = 0.4$
45	2-1-2	0.8525	0.9221	1.0107	1.1283	1.6144	1.6928	1.7883	1.9100
	1-1-1	0.8607	0.9339	1.0283	1.1562	1.6015	1.6778	1.7713	1.8918
	2-2-1	0.8907	0.9741	1.0868	1.2504	1.5934	1.6561	1.7322	1.8312
	1-8-1	0.8891	0.9636	1.0607	1.1951	1.6648	1.7271	1.7999	1.8891
65	2-1-2	1.7718	1.9165	2.1006	2.3452	1.6121	1.6899	1.7847	1.9052
	1-1-1	1.7881	1.9400	2.1361	2.4017	1.5991	1.6747	1.7673	1.8864
	2-2-1	1.8469	2.0190	2.2516	2.5891	1.5908	1.6527	1.7274	1.8238
	1-8-1	1.8442	1.9980	2.1987	2.4760	1.6628	1.7244	1.7963	1.8839
80	2-1-2	2.6806	2.8995	3.1781	3.5482	1.6114	1.689	1.7835	1.9036
	1-1-1	2.7049	2.9347	3.2313	3.6332	1.5983	1.6737	1.766	1.8846
	2-2-1	2.7922	3.0521	3.4032	3.9126	1.5900	1.6516	1.7259	1.8214
	1-8-1	2.7885	3.0208	3.3237	3.7424	1.6621	1.7236	1.7951	1.8822
100	2-1-2	4.1849	4.5266	4.9615	5.5394	1.6108	1.6883	1.7827	1.9025
	1-1-1	4.2225	4.5811	5.0441	5.6714	1.5978	1.673	1.7651	1.8834
	2-2-1	4.3569	4.762	5.3093	6.1032	1.5894	1.6508	1.7248	1.8197
	1-8-1	4.3514	4.7135	5.1858	5.8385	1.6617	1.7230	1.7943	1.8810

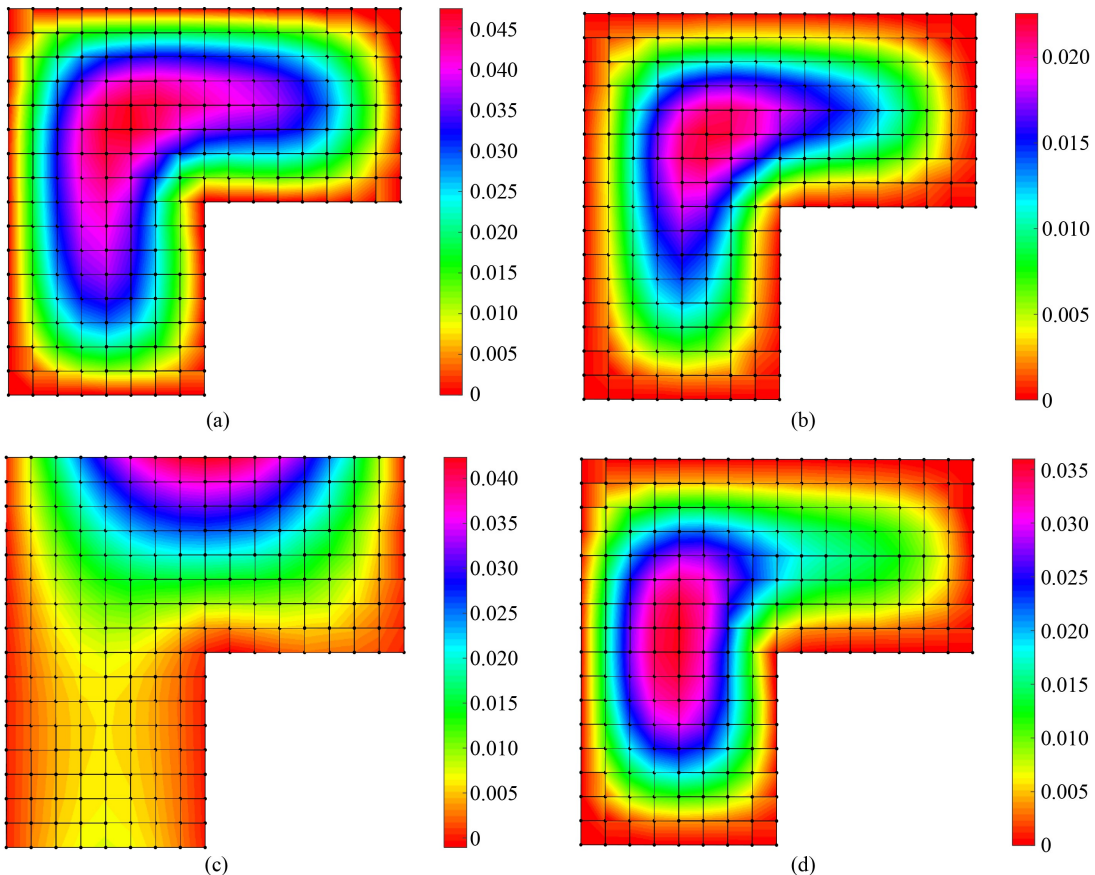


Fig. 15 Deformation field of FGP L-shape sandwich plates (top view) (scheme 1-1-1; $h/a = 10$; $k = 1$; $\xi = 0.2$). (a) The SSSSS FGP L-shape sandwich plate; (b) the CCCCCC FGP L-shape sandwich plate; (c) the SFSFSF FGP L-shape sandwich plate; (d) the SCSCSC FGP L-shape sandwich plate.

smaller than those of L-shape sandwich plates with other BCs because the clamped boundary condition is less flexible than the simply supported and free BCs.

5 Conclusions

This paper proposes a Q4 finite element with nine DOFs per node for the investigation of the static response of FGP sandwich plates including L-shape models. The finite element formulation based on Quasi-3D theory helps to describe more accurately the stress-strain field of plates, especially with thick plates. Besides, the use of Quasi-3D theory satisfies the stress-free condition at the upper and lower boundaries of plates condition and does not require use of any anti “shear-locking” techniques. The paper also analyses and discusses the effects of geometrical parameters, material properties on the static response of FGP sandwich plates consisting of L-shape models. From the formulas and obtained numerical results, some main conclusions can be highlighted as follows.

1) Using the Q4 element combined with Quasi-3D theory easily discretizes the problem domain even with complex geometric domains and avoids “the shear-locking” phenomenon that appears in the classical Q4 element.

2) Using sandwich structures with an FGP core not only reduces the overall mass but also increases the flexural strength of the structure in some specific cases.

3) The material properties such as power-law index k , porosity coefficient ξ and geometric parameters such as length-thickness ratios, thickness ratio between the bottom layer significantly affect the static bending of FGP sandwich plates. In general, power-law index k and porosity coefficient ξ make reduce the plate's stiffness. Moreover, adjusting these parameters can help control the stiffness of sandwich plates as desired.

4) The numerical results provided are useful for calculations for design of FGP sandwich plates in engineering practice.

References

1. Vo T P, Thai H T, Nguyen T K, Maher A, Lee J. Finite element model for vibration and buckling of functionally graded sandwich beams based on a refined shear deformation theory. *Engineering Structures*, 2014, 64: 12–22
2. Asghari M, Ahmadian M T, Kahrobaiany M H, Rahaeifard M. On the size-dependent behavior of functionally graded micro-beams. *Materials & Design*, 2010, 31(5): 2324–2329
3. Trinh L C, Vo T P, Osofere A I, Lee J. Fundamental frequency analysis of functionally graded sandwich beams based on the state space approach. *Composite Structures*, 2016, 156: 263–275
4. Vo T P, Thai H T, Nguyen T K, Inam F. Static and vibration analysis of functionally graded beams using refined shear deformation theory. *Meccanica*, 2014, 49(1): 155–168
5. Reddy J. Analysis of functionally graded plates. *International Journal for Numerical Methods in Engineering*, 2000, 47(1–3): 663–684
6. Luat D T, Van Thom D, Thanh T T, Van Minh P, Van Ke T, Van Vinh P. Mechanical analysis of bi-functionally graded sandwich nanobeams. *Advances in Nano Research*, 2021, 11: 55–71
7. Nguyen V H, Nguyen T K, Thai H T, Vo T P. A new inverse trigonometric shear deformation theory for isotropic and functionally graded sandwich plates. *Composites. Part B, Engineering*, 2014, 66: 233–246
8. Zenkour A M. Generalized shear deformation theory for bending analysis of functionally graded plates. *Applied Mathematical Modelling*, 2006, 30(1): 67–84
9. Li S, Zheng S, Chen D. Porosity-dependent isogeometric analysis of bi-directional functionally graded plates. *Thin-walled Structures*, 2020, 156: 106999
10. Tran T T, Le P B. Nonlocal dynamic response analysis of functionally graded porous L-shape nanoplates resting on elastic foundation using finite element formulation. *Engineering with Computers*, 2022, 1–17
11. Zhao X, Lee Y, Liew K M. Free vibration analysis of functionally graded plates using the element-free kp-Ritz method. *Journal of Sound and Vibration*, 2009, 319(3–5): 918–939
12. Nguyen-Xuan H, Tran L V, Nguyen-Thoi T, Vu-Do H. Analysis of functionally graded plates using an edge-based smoothed finite element method. *Composite Structures*, 2011, 93(11): 3019–3039
13. Nguyen H N, Canh T N, Thanh T T, Ke T V, Phan V D, Thom D V. Finite element modelling of a composite shell with shear connectors. *Symmetry*, 2019, 11(4): 527
14. Karamanli A, Vo T P. Size dependent bending analysis of two directional functionally graded microbeams via a quasi-3D theory and finite element method. *Composites. Part B, Engineering*, 2018, 144: 171–183
15. Thai C H, Zenkour A M, Abdel Wahab M, Nguyen-Xuan H. A simple four-unknown shear and normal deformations theory for functionally graded isotropic and sandwich plates based on isogeometric analysis. *Composite Structures*, 2016, 139: 77–95
16. Tran T T, Pham Q H, Nguyen-Thoi T. Static and free vibration analyses of functionally graded porous variable-thickness plates using an edge-based smoothed finite element method. *Defence Technology*, 2021, 17(3): 971–986
17. Tran T T, Nguyen P C, Pham Q H. Vibration analysis of FGM plates in thermal environment resting on elastic foundation using ES-MITC3 element and prediction of ANN. *Case Studies in Thermal Engineering*, 2021, 24: 100852
18. Tran T T, Pham Q H, Nguyen-Thoi T. Dynamic analysis of functionally graded porous plates resting on elastic foundation taking into mass subjected to moving loads using an edge-based smoothed finite element method. *Shock and Vibration*, 2020, 2020: 8853920
19. Pham Q H, Tran V K, Tran T T, Nguyen-Thoi T, Nguyen P C, Pham V D. A nonlocal quasi-3D theory for thermal free vibration analysis of functionally graded material nanoplates resting on

- elastic foundation. *Case Studies in Thermal Engineering*, 2021, 26: 101170
20. Pham Q H, Thanh Tran T, Ke Tran V, Nguyen P C, Nguyen-Thoi T. Free vibration of functionally graded porous non-uniform thickness annular-nanoplates resting on elastic foundation using ES-MITC3 element. *Alexandria Engineering Journal*, 2022, 61(3): 1788–1802
 21. Pham Q H, Tran T T, Tran V K, Nguyen P C, Nguyen-Thoi T, Zenkour A M. Bending and hygro-thermo-mechanical vibration analysis of a functionally graded porous sandwich nanoshell resting on elastic foundation. *Mechanics of Advanced Materials and Structures*, 2021, 1–21
 22. Thanh T T, Van Ke T, Hoa P Q, Trung N T. An edge-based smoothed finite element for buckling analysis of functionally graded material variable-thickness plates. *Vietnam Journal of Mechanics*, 2021, 43: 221–235
 23. Nguyen P C, Pham Q H, Tran T T, Nguyen-Thoi T. Effects of partially supported elastic foundation on free vibration of FGP plates using ES-MITC3 elements. *Ain Shams Engineering Journal*, 2022, 13(3): 101615
 24. Tran T T, Pham Q H, Nguyen-Thoi T. An edge-based smoothed finite element for free vibration analysis of functionally graded porous (FGP) plates on elastic foundation taking into mass (EFTIM). *Mathematical Problems in Engineering*, 2020, 2020: 8278743
 25. Sobhy M. A comprehensive study on FGM nanoplates embedded in an elastic medium. *Composite Structures*, 2015, 134: 966–980
 26. Tornabene F. Free vibration analysis of functionally graded conical, cylindrical shell and annular plate structures with a four-parameter power-law distribution. *Computer Methods in Applied Mechanics and Engineering*, 2009, 198(37–40): 2911–2935
 27. Mantari J L. Refined and generalized hybrid type quasi-3D shear deformation theory for the bending analysis of functionally graded shells. *Composites. Part B, Engineering*, 2015, 83: 142–152
 28. Torabi J, Kiani Y, Eslami M R. Linear thermal buckling analysis of truncated hybrid FGM conical shells. *Composites. Part B, Engineering*, 2013, 50: 265–272
 29. Rezaei A, Saidi A. Application of Carrera Unified Formulation to study the effect of porosity on natural frequencies of thick porous–cellular plates. *Composites. Part B, Engineering*, 2016, 91: 361–370
 30. Rezaei A, Saidi A. Exact solution for free vibration of thick rectangular plates made of porous materials. *Composite Structures*, 2015, 134: 1051–1060
 31. Zhao J, Xie F, Wang A, Shuai C, Tang J, Wang Q. A unified solution for the vibration analysis of functionally graded porous (FGP) shallow shells with general boundary conditions. *Composites. Part B, Engineering*, 2019, 156: 406–424
 32. Zhao J, Xie F, Wang A, Shuai C, Tang J, Wang Q. Vibration behavior of the functionally graded porous (FGP) doubly-curved panels and shells of revolution by using a semi-analytical method. *Composites. Part B, Engineering*, 2019, 157: 219–238
 33. Li Q, Wu D, Chen X, Liu L, Yu Y, Gao W. Nonlinear vibration and dynamic buckling analyses of sandwich functionally graded porous plate with graphene platelet reinforcement resting on Winkler–Pasternak elastic foundation. *International Journal of Mechanical Sciences*, 2018, 148: 596–610
 34. Sahmani S, Aghdam M M, Rabczuk T. Nonlocal strain gradient plate model for nonlinear large-amplitude vibrations of functionally graded porous micro/nano-plates reinforced with GPLs. *Composite Structures*, 2018, 198: 51–62
 35. Guo H, Zhuang X, Chen P, Alajlan N, Rabczuk T. Stochastic deep collocation method based on neural architecture search and transfer learning for heterogeneous porous media. *Engineering with Computers*, 2022, 1–26
 36. Guo H, Zhuang X, Chen P, Alajlan N, Rabczuk T. Analysis of three-dimensional potential problems in non-homogeneous media with physics-informed deep collocation method using material transfer learning and sensitivity analysis. *Engineering with Computers*, 2022, 1–22
 37. Zhuang X, Guo H, Alajlan N, Zhu H, Rabczuk T. Deep autoencoder based energy method for the bending, vibration, and buckling analysis of Kirchhoff plates with transfer learning. *European Journal of Mechanics. A, Solids*, 2021, 87: 104225
 38. Guo H, Zheng H, Zhuang X. Numerical manifold method for vibration analysis of Kirchhoff's plates of arbitrary geometry. *Applied Mathematical Modelling*, 2019, 66: 695–727
 39. Guo H, Zheng H. The linear analysis of thin shell problems using the numerical manifold method. *Thin-walled Structures*, 2018, 124: 366–383
 40. Zenkour A. A comprehensive analysis of functionally graded sandwich plates: Part 1—Deflection and stresses. *International Journal of Solids and Structures*, 2005, 42(18–19): 5224–5242
 41. Zenkour A M. The effect of transverse shear and normal deformations on the thermomechanical bending of functionally graded sandwich plates. *International Journal of Applied Mechanics*, 2009, 1(4): 667–707
 42. Zenkour A, Alghamdi N. Bending analysis of functionally graded sandwich plates under the effect of mechanical and thermal loads. *Mechanics of Advanced Materials and Structures*, 2010, 17(6): 419–432
 43. Zenkour A, Sobhy M. Thermal buckling of various types of FGM sandwich plates. *Composite Structures*, 2010, 93(1): 93–102
 44. Zenkour A, Alghamdi N. Thermomechanical bending response of functionally graded nonsymmetric sandwich plates. *Journal of Sandwich Structures & Materials*, 2010, 12(1): 7–46
 45. Zenkour A M. Bending analysis of functionally graded sandwich plates using a simple four-unknown shear and normal deformations theory. *Journal of Sandwich Structures & Materials*, 2013, 15(6): 629–656
 46. Daikh A A, Zenkour A M. Free vibration and buckling of porous power-law and sigmoid functionally graded sandwich plates using a simple higher-order shear deformation theory. *Materials Research Express*, 2019, 6(11): 115707
 47. Zenkour A. A comprehensive analysis of functionally graded sandwich plates: Part 2—Buckling and free vibration. *International Journal of Solids and Structures*, 2005, 42(18–19): 5243–5258
 48. Daikh A A, Zenkour A M. Effect of porosity on the bending analysis of various functionally graded sandwich plates. *Materials Research Express*, 2019, 6(6): 065703
 49. Zenkour A M. A quasi-3D refined theory for functionally graded single-layered and sandwich plates with porosities. *Composite*

- Structures, 2018, 201: 38–48
- 50. Thai H T, Nguyen T K, Vo T P, Lee J. Analysis of functionally graded sandwich plates using a new first-order shear deformation theory. *European Journal of Mechanics. A, Solids*, 2014, 45: 211–225
 - 51. Sid Ahmed Houari M, Tounsi A, Anwar Bég O. Thermoelastic bending analysis of functionally graded sandwich plates using a new higher order shear and normal deformation theory. *International Journal of Mechanical Sciences*, 2013, 76: 102–111
 - 52. Nguyen T K, Nguyen V H, Chau-Dinh T, Vo T P, Nguyen-Xuan H. Static and vibration analysis of isotropic and functionally graded sandwich plates using an edge-based MITC3 finite elements. *Composites. Part B, Engineering*, 2016, 107: 162–173
 - 53. Pham Q H, Nguyen P C, Tran T T, Nguyen-Thoi T. Free vibration analysis of nanoplates with auxetic honeycomb core using a new third-order finite element method and nonlocal elasticity theory. *Engineering with Computers*, 2021, 1–19
 - 54. Li D, Deng Z, Xiao H, Zhu L. Thermomechanical bending analysis of functionally graded sandwich plates with both functionally graded face sheets and functionally graded cores. *Mechanics of Advanced Materials and Structures*, 2018, 25(3): 179–191
 - 55. Li D, Deng Z, Xiao H, Jin P. Bending analysis of sandwich plates with different face sheet materials and functionally graded soft core. *Thin-walled Structures*, 2018, 122: 8–16
 - 56. Tounsi A, Houari M S A, Benyoucef S, Adda Bedia E A. A refined trigonometric shear deformation theory for thermoelastic bending of functionally graded sandwich plates. *Aerospace Science and Technology*, 2013, 24(1): 209–220
 - 57. Tlidji Y, Daouadji T H, Hadji L, Tounsi A, Bedia E A A. Elasticity solution for bending response of functionally graded sandwich plates under thermomechanical loading. *Journal of Thermal Stresses*, 2014, 37(7): 852–869
 - 58. Zaoui F Z, Ouinas D, Tounsi A. New 2D and quasi-3D shear deformation theories for free vibration of functionally graded plates on elastic foundations. *Composites. Part B, Engineering*, 2019, 159: 231–247
 - 59. Neves A, Ferreira A, Carrera E, Cinefra M, Roque C, Jorge R, Soares C M. Static, free vibration and buckling analysis of isotropic and sandwich functionally graded plates using a quasi-3D higher-order shear deformation theory and a meshless technique. *Composites. Part B, Engineering*, 2013, 44(1): 657–674
 - 60. Farzam-Rad S A, Hassani B, Karamodin A. Isogeometric analysis of functionally graded plates using a new quasi-3D shear deformation theory based on physical neutral surface. *Composites. Part B, Engineering*, 2017, 108: 174–189
 - 61. Vafakhah Z, Navayi Neya B. An exact three dimensional solution for bending of thick rectangular FGM plate. *Composites. Part B, Engineering*, 2019, 156: 72–87
 - 62. Vo T P, Thai H T, Nguyen T K, Inam F, Lee J. A quasi-3D theory for vibration and buckling of functionally graded sandwich beams. *Composite Structures*, 2015, 119: 1–12
 - 63. Reddy J N. *Mechanics of Laminated Composite Plates and Shells: Theory and Analysis*. Boca Raton: CRC press, 2003
 - 64. Sobhy M. An accurate shear deformation theory for vibration and buckling of FGM sandwich plates in hygrothermal environment. *International Journal of Mechanical Sciences*, 2016, 110: 62–77
 - 65. Touratier M. An efficient standard plate theory. *International Journal of Engineering Science*, 1991, 29(8): 901–916
 - 66. Soldatos K P. A transverse shear deformation theory for homogeneous monoclinic plates. *Acta Mechanica*, 1992, 94(3–4): 195–220
 - 67. Karama M, Afaq K, Mistou S. Mechanical behaviour of laminated composite beam by the new multi-layered laminated composite structures model with transverse shear stress continuity. *International Journal of Solids and Structures*, 2003, 40(6): 1525–1546
 - 68. Mahi A, Adda Bedia E A, Tounsi A. A new hyperbolic shear deformation theory for bending and free vibration analysis of isotropic, functionally graded, sandwich and laminated composite plates. *Applied Mathematical Modelling*, 2015, 39(9): 2489–2508
 - 69. Pham Q H, Nguyen P C, Thanh Tran T. Dynamic response of porous functionally graded sandwich nanoplates using nonlocal higher-order isogeometric analysis. *Composite Structures*, 2022, 290: 115565
 - 70. Vasiraja N, Nagaraj P. The effect of material gradient on the static and dynamic response of layered functionally graded material plate using finite element method. *Bulletin of the Polish Academy of Sciences. Technical Sciences*, 2019, 67(4): 827–838